CHAPTER 2 – MEASURING AND PREDICTING RELATIVE HUMIDITY AND TEMPERATURE PROFILE DISTRIBUTIONS INSIDE RAILROAD CONCRETE CROSSTIES

2.1 Acknowledgement

The development of this chapter is accomplished with field testing carried out in two locations: Rantoul, IL, and Lytton, BC, Canada. Researchers at the University of British Columbia, Okanagan, supported the project by collecting field data on behalf of the author in Lytton, BC, Canada. For that, I am very grateful to Professors Gord Lovegrove and Ahmad Rteil, and to students Trevor Billows and Kyle Stratton. Additionally, I am grateful to industrial partner Jim Parsley and staff at LB Foster CXT Concrete Ties where numerous crossties were instrumented during the manufacturing process for this study.

2.2 Abstract

Concrete crossties (alternatively known as ties or sleepers) are subjected to a wide range of climatic conditions across North America. Among these environments are those that include cyclic freezing and thawing air temperatures. In conventional concrete, freeze-thaw cyclic damage is mitigated by chemically entraining microscopically-sized air bubbles in the fresh concrete. These empty air voids in hardened concrete allow for hydraulic pressures to be alleviated during freezing events. In high performance concrete, however, the low water-to-cementitious ratio and pozzolanic mineral admixtures can result in a highly impermeable microstructure that may not allow for an increase of liquid moisture to a critical level (86-88%) in which freeze-thaw damage would occur. As a consequence, high performance concrete crossties may be freeze-thaw resistant without the incorporation of chemically entrained air. In order to better understand the appropriateness of air-entrainment in high performance concrete crossties, several concrete crossties were instrumented with hygrothermal sensors during manufacturing. These concrete crossties were installed in track in Lytton, British Columbia, Canada, and in model ballast in Rantoul, Illinois, United States. The internal relative humidity and temperature of the concrete crossties and complementary concrete beams, as well as ambient readings in air and ballast, were observed for a time span of one year. Predictive models based on half-space approximations are

applied in order to predict the concrete crosstie internal profiles of relative humidity and temperature. It is found that modifications to boundary conditions at the top surface (at the rail seat area) improves the predictive fit to the experimental data, which suggests that internal relative humidity and temperature profiles can be predicted utilizing these modifications to the boundary conditions and environmental weather data alone.

2.3 Introduction and Background

2.3.1 Deterioration of railroad concrete crossties

Concrete crossties have been replacing timber ties over the last several decades because of the ability of concrete crossties to sustain higher freight loads, higher train speeds, and have reduced maintenance costs [Zeman, 2010]. However, early-age deterioration can render the last point moot if premature material damage necessitates repair or replacement of the concrete crosstie. Concrete crossties are typically manufactured in precast plants and are additionally pre-stressed for enhanced mechanical performance. As a result, concrete crossties manufactured in the United States in the 1970s with steam curing often suffered deterioration mechanisms like delayed ettringite formation [Tepponen and Eriksson, 1987; Ferdous and Manalo, 2014]. However, present-day concrete crossties are manufactured without steam curing and incorporate new chemical admixtures not previously available to manufacturers. These chemical (and mineral) admixtures have led to the development of high performance concrete that is highly flowable. However, new early-age deterioration mechanisms have become apparent, which is of great concern to the Federal Railroad Administration (FRA) as the United States continues to move toward the construction of a national high speed rail network that implement these high performance concrete crossties.

Early-age deterioration mechanisms of concrete crossties are generally structural (abrasion, crushing, e.g.) and material (cavitation erosion, hydraulic pressure, e.g.) in nature [Ferdous and Manalo, 2014]. These damages can additionally be affected by frost heaving (the action in which water in fouled ballast freezes leading to large-scale upheaval of concrete crossties) [Hakon, 1978]. It is also possible for freeze-thaw damage to occur within the concrete crosstie since the material is exposed to outdoor environments. In particular, freeze-thaw damage can be problematic at the

rail seat area where the confined geometry of the concrete crosstie, pad, clips, shoulder, and rail line converge. The highly confined rail seat area possibly leads to pooling of water from precipitation (rain or melting snow) which can lead to absorption of water, scaling, and freeze-thaw damage at low temperatures [Bakharev and Struble, 1997]. However, recent research has demonstrated that freeze-thaw damage is exacerbated above critical levels of saturation higher than 86-88% [Li *et al.*, 2012]. As such, it is necessary to gain a better understanding of moisture levels and freezing temperatures inside concrete crossties to better assess their freeze-thaw damage potential.

2.3.2 One-dimensional modeling of internal relative humidity distribution

Simulating the extent of moisture and temperature gradients within concrete is highly sought in pavement engineering because of moisture and thermal curling of slabs, which leads to durability issues. As such, infinite halfspace solutions exist for pavements. In this study, two halfspace solutions to predict relative humidity and temperature distributions are applied to concrete crossties. Limitations to this 1-dimensional modeling approach is discussed in greater detail in later sections. Figure 2-1 shows the simplified approach of a 3-dimensional concrete crossties in aggregate ballast overlayed by a polyurethane pad and steel rail as a series of stacked, infinite halfspaces.

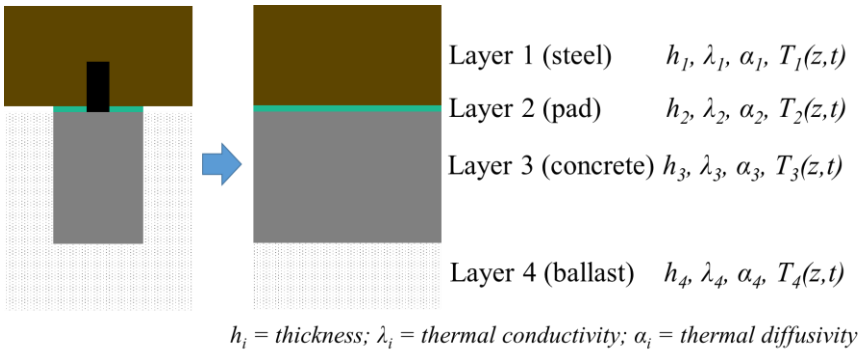

Figure 2-1 Depiction of a concrete crosstie at the rail seat area (left) where the steel rail line, polyurethane pad, concrete crosstie, and aggregate ballast are depicted as layered, infinite halfspaces (right).

Relative humidity can be modeled by the 1-dimensional moisture transport equation [Kim and Lee, 1999]

$$\frac{\partial RH(t,z)}{\partial t} = div(D \cdot grad(RH(t,z))) - \frac{\partial RH_S(t,z)}{\partial t} \qquad \text{Equation 2-1}$$

where *RH* is a function of time (sec), *t*, and depth (m), *z*; $\frac{\partial RH_S(t,z)}{\partial t}$ is the change in relative humidity due to hydration for early-age concrete (assumed as $\frac{\partial RH_S(t,z)}{\partial t} = 0$ for hardened concrete; and *D* is the moisture diffusivity, which is a function of both internal relative humidity and concrete porosity. The moisture diffusivity factor is non-linear (where at low RH, vapor- and gas-pressure gradients govern transport properties while at high RH, capillary suction governs transport properties). The moisture diffusivity can be expressed by an effective diffusivity [Bažant and Najjar, 1972]

$$D = D_o \left(\alpha_o \frac{1-\alpha_o}{1+\left(1-RH/_{1-RH_c}\right)^n} \right) \qquad \text{Equation 2-2}$$

where D_o (m^2/s) is the moisture diffusivity at complete saturation; *n* is a regression coefficient ranging from 6 to 16 for concrete [Leech *et al.*, 2003]; $\alpha_o = D_1/D_o$, where D_1 is the diffusivity at 0% RH; and RH_c is the bifurcate point above which capillary suction governs (typically 75 to 80%) [Qin and Hiller, 2014]. The moisture diffusivity at complete saturation can be related to the water-to-cementitious ratio as shown in Table 2-1.

Table 2-1 Moisture diffusivity at saturation estimated from w/c ratio (from [1]Kang *et al.*, 2012, and [2]Qin and Hiller, 2014).

w/c	D_o (10^{-6} m^2/hour)[1]	D_o (10^{-6} m^2/hour)[2]
0.28	2.02	0.68
0.40	2.10	1.59
0.50	2.26	-
0.68	2.87	2.57

The boundary conditions are defined at the top and underside of the crosstie by two hygrochron sensors installed within the ballast. The boundary condition at the top of the crosstie is modified in order to better represent wetting events due to precipitation (rain or melting snow). Table 2-2 shows weather conditions which increase the measured relative humidity value to 100% RH over a given time frame.

Table 2-2 Modified boundary condition at the top of concrete crossties and beams as subject to reported weather conditions (adapted from Qin and Hiller, 2014).

Reported Weather Condition	**Modified Wetting Duration**
Drizzle	RH_{upper} = 100 % for 1 hour
Fog	
Mist	
Light Rain	RH_{upper} = 100 % for 4 hours
Light Thunderstorms and Rain	
Thunderstorms and Rain	RH_{upper} = 100 % for 8 hours
Rain	
Heavy Thunderstorms and Rain	RH_{upper} = 100 % for 10 hours
Heavy Rain	
Light Snow	
Snow	RH_{upper} = 100 % for 15 hours
Heavy Snow	RH_{upper} = 100 % for 20 hours

Equation 2-1 is iteratively solved in MatLab until the *RH (t)* converges to within 1% RH.

2.3.3 One-dimensional modeling of internal temperature distribution

Several models exist to predict the temperature distribution inside concrete pavements [Barber, 1957; Dempsey and Thompson, 1970; Solaimanian and Kennedy, 1993]. Dempsey and Thompson's model is well regarded for long-term pavement temperature predictions. However, modeling a concrete crosstie presents two challenges: it is 3-dimensional and multi-layered. Adopting a closed-form solution, thusly, yields an incorrect representation of the crosstie at its exterior edges. However, a first-principles understanding can be pursued where the suitability of a 1-dimensional model can be evaluated for use in predicted concrete crosstie internal temperature distributions.

Wang and Roesler [2014] proposed a separation of variables method to predict the internal temperature profile, $T_i\ (z,t)$, inside a multi-layered rigid pavement system. A 1-dimensional heat transfer problem is modeled using

$$\frac{\partial T_i}{\partial t}(z,t) = \alpha_i \frac{\partial^2 T_i}{\partial z^2}(z,t) \qquad \text{Equation 2-3}$$

where α_i is the thermal diffusivity coefficient (m^2/h); $H_{i-1} < z < H_i$ is the cumulative depth through the multi-layered system (m); $H_i = \sum_{k=1}^{i} h_k$ is the individual thickness of each layer (m); i = 1, 2,

…, $n-1$ are individual layers where $H_0 = 0$ and $H_n = \infty$; and $n \geq 4$ is the number of layers required in this analysis.

Two boundary conditions constrain the final solution to be continuous along the intermediary interfaces between any consecutive layers:

$$T_i(H_i, t) = T_{i+1}(H_i, t) \qquad \text{Equation 2-4}$$

$$\lambda_i \frac{\partial T_i}{\partial t}(H_i, t) = \lambda_{i+1} \frac{\partial T_{i+1}}{\partial z}(H_i, t) \qquad \text{Equation 2-5}$$

where λ_i is the thermal conductivity coefficient (kcal/m h ^oC). The third boundary condition is an energy balance between the surface of the concrete and environmental conditions

$$-\lambda_i \frac{\partial T_i}{\partial t}(0, t) = a_s Q(t) - F(t) + B[T_a(t) - T_1(0, t)] \qquad \text{Equation 2-6}$$

where a_s is the surface material absorptivity relative to the solar radiation (unitless); $Q(t)$ is the solar radiation flux (kcal / m^2 h) at time t (hour); $F(t)$ is the irradiation flux emitted by the pavement surface (kcal / m^2 h ^oC); B is the surface material convection coefficient (kcal / m^2 h ^oC); and $T_a(t)$ is the ambient air temperature (^oC) at time t (hour). Continuous functions of $Q(t)$ and $T_a(t)$ are desired in order to produce a closed-form final solution, so an interpolatory trigonometric set of polynomials using the least squares approximation can be used [Burden and Faires, 2001; Wang and Roesler, 2014]. By incorporating these trigonometric polynomials and simplifying the irradiation energy by a factor of 1/3 [Barber, 1957], then Equation 2-6 can be written in the compact form

$$-\lambda_i \frac{\partial T_i}{\partial t}(0, t) = B[\sum_{i=1}^{2m} A_i \sin(\omega_i t + \phi_i) - T_1(0, t)] \qquad \text{Equation 2-7}$$

where $2m$ is the number of sub-intervals used to create the interpolatory trigonometric set of polynomials; and A_i, ω_i, and ϕ_i are mathematical representations of amplitude, frequency, and phase angle, respectively, and are defined elsewhere [Wang and Roesler, 2014].

Wang and Roesler observe that the sinusoidal term $\sin(w_i t + \phi_i)$ can be related to the complex number $e^{j(\omega t + \phi)}$ via the Euler formula where $j^2 = -1$. As such, the complex-valued

function can be solved where the imaginary final solution corresponds to the real solution for the 1D temperature profile $T_i(z,t)$. Because the principle of superposition is applied k times in order to solve the complex-valued function, the individual solutions of $T_{ik}(z,t)$ must be summed across the k-th index in order to yield the final solution for the n-th layered temperature profile distribution. The solution from one iteration of solving the imaginary part of the complex-valued function are

$$T_{ik}(z,t) = \Delta_{11} e^{-\upsilon_1 z} \sin(\omega t - \upsilon_i z + \delta_{11} + \phi) + \Delta_{12} e^{\upsilon_1 z} \sin(\omega t + \upsilon_i z + \delta_{12} + \phi) \quad \text{Equation 2-8}$$

for $0 \leq z \leq H_1$;

$$T_{ik}(z,t) = \Delta_{i1} e^{H_{i-1}\upsilon_{i-1} + \upsilon_i (H_{i-1} - z)} \sin(\omega t - \upsilon_i z + \delta_{i1} + \phi) + \Delta_{i2} e^{H_{i-1}\upsilon_{i-1} - \upsilon_i (H_{i-1} - z)} \sin(\omega t + \upsilon_i z + \delta_{12} + \phi) \quad \text{Equation 2-9}$$

for $H_{i-1} \leq z \leq H_i$, and $i = 2, 3, \ldots, n-1$; and

$$T_{nk}(z,t) = \Delta_n e^{H_{n-1}\upsilon_{n-1} + \upsilon_n (H_{n-1} - z)} \sin(\omega t - \upsilon_n z + \delta_{n1} + \phi) \quad \text{Equation 2-10}$$

for $z \geq H_{n-1}$. The variables Δ_{i1}, δ_{i1} for $i = 1, 2, \ldots, n$ and Δ_{i2}, δ_{12} for $i = 1, 2, \ldots, n-1$ in Equations 2-8 through 2-10 are defined elsewhere [Wang and Roesler, 2014].

2.3.4 Estimating solar radiation as an input for the one-dimensional temperature model

The predictive temperature model requires two input parameters in order to predict the internal temperature profile distribution inside concrete: ambient air temperature and solar radiation. Although ambient air temperature is available in many locations from meteorological data, solar radiation is not as readily available and is prone to incomplete data sets [Al Riza *et al.*, 2011]. Solar radiation estimation is employed within agricultural disciplines in order understand soil temperature and soil moisture conditions. As such, a number of different estimations exist throughout the literature [Monteith, 1965; Bristow and Campbell, 1984; Hargreaves and Samani, 1985; Liu, 1996; McVicar and Jupp, 1999] for solar radiation with varying degrees of simplicity.

Spokas and Forcella [2006] estimate incoming solar radiation as affected by changing weather conditions and changing geo-temporal attributes at a given location. Their model is advantageous because it is sensitive to changing hourly conditions as opposed to other models

which only account for mean daily fluctuations and site-calibration. In their model, they assume that total incoming solar radiation, Q_T, is divided into two components

$$Q_T = Q_B + Q_D \qquad \text{Equation 2-11}$$

where Q_B is direct beam radiation and Q_D is indirect, diffuse radiation. Direct beam radiation is transmitted parallel to the sun's rays (zenith angle) and is dependent upon the location on Earth, the time of day, the time of year, and the extent of transmittance through the atmosphere. Direct beam radiation is assumed to be [Liu and Jordan, 1960]

$$Q_B = Q_{Bo}\tau^m \qquad \text{Equation 2-12}$$

where Q_{Bo} is the solar constant (1,360 W/m^2), τ is the atmospheric transmittance, and m is the optical air mass number. The optical air mass number is a function of atmospheric pressure, zenith angle, and elevation of the site [Campbell and Norman, 1998]. Indirect, diffuse radiation is reflected or absorbed in the atmosphere, clouds, or dust and a fraction of this radiation is scattered toward the surface of Earth. It is assumed to be [Liu and Jordan, 1960]

$$Q_D = 0.30(1 - \tau^m)Q_{Bo}cos\Psi \qquad \text{Equation 2-13}$$

where Ψ is the zenith angle in radians. The zenith angle is dependent upon the latitude of the site, standard time, time at solar noon, and calendar day [Campbell and Jordan, 1998]. Figure 2-2 depicts the direct beam and diffuse solar radiation emanating from the sun, transmitting and reflecting through clouds and the atmosphere, and cumulatively hitting the top surface of the (simplified) multi-layered concrete crosstie system.

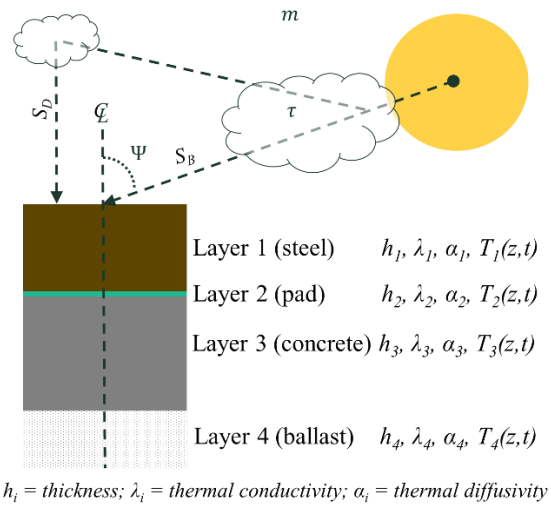

Figure 2-2 Depiction of a concrete crosstie at the rail seat area where the steel rail line, polyurethane pad, concrete crosstie, and aggregate ballast are depicted as layered, infinite halfspaces.

2.4 Significance of Research

Concrete crossties, like any outdoor concrete structure, are susceptible to freeze-thaw damage, yet the distribution of internal liquid moisture within concrete crossties is not well understood. In particular, the state of liquid moisture at the rail seat area is complicated due to the configuration of the rail line, pad, clips, and shoulders. This study aims to enhance the concrete crosstie industry's understanding of freeze-thaw susceptibility by measuring the internal relative humidity and temperature of instrumented crossties installed in track. Additionally, the results of this study can be compared against current standard tests in order to achieve improved environmental design criteria for concrete crosstie freeze-thaw damage.

2.5 Experimental Methods

2.5.1 Sensor type and preparation of installation method

Hygrochron sensors, able to measure both relative humidity and temperature, called iButtons (DS1923-F5) were selected because of each sensor's ability to record data and operate under battery-power. These benefits eliminated the need to devise an external data-acquisition support system. For relative humidity measurements, the sensors make use of two electrodes joined by a capacitive film. When water vapor accumulates onto the film, then the dielectric constant, κ,

measured between the two electrodes changes in a linear relationship. As such, a linear relationship can be established by experimentally measuring the dielectric constant with respect to changing relative humidity in controlled environments.

The sensors execute software correction algorithms for both relative humidity and temperature measurements based on the conversion of 8-bit or 16-bit data formats to decimal formats [Maxim Integrated, 2013]. Additionally, whenever a capacitive film is exposed to high relative humidity environments (greater than 70% RH, e.g.), for extended periods of time, then the reading may become affected in a phenomenon known as *saturation drift*. It is possible to account for this saturation drift by correcting the measured relative humidity value, RH_N, at the Nth hour the device has been continuously exposed to 70% RH and higher (or 20% RH and lower) with the following expression

$$RH_{saturation\ drift\ corrected} = RH_N - \sum_{k=1}^{N} \frac{(0.0156)(\overline{RH_k})(2.54^{-0.3502k})}{1+{}^{(\overline{T_k}-25)}/_{100}} \quad \text{Equation 2-14}$$

where RH_N is the relative humidity at the end of the Nth hour when the device is exposed to high or low relative humidity, $\overline{RH_k}$ is the average relative humidity through the kth hour that that device has been exposed to high or low relative humidity, and $\overline{T_k}$ is the average temperature (in Celsius) through the kth hour the device has been continuously exposed to high or low relative humidity. The numbers in the equation are empirical and are derived from curve-fitted data sets [Maxim Integrated, 2013].

The sensors were fitted into iButton retainers (DS9098P) which introduced soldering points for wiring. Multi-conductor shielded cabling was soldered onto the retainer in order to enable remote communication with each individual sensor. The sensor and retainer were fitted inside of a plastic dip coated eye bolt which was additionally affixed onto a steel angle bracket with unthreaded holes spaced one inch apart (see Figure 2-3). Eleven individual brackets with 2-inch nominal spacing (see Figure 2-4) were constructed. A single layer of GORE-TEX fabric (a fabric that allows water vapor to pass through but not liquid water) was wrapped around each sensor in order to protect the wiring connections.

Figure 2-3 Construction of iButton sensors (left), fitted with rubber bands (center), and covered in GORE-TEX fabric (right).

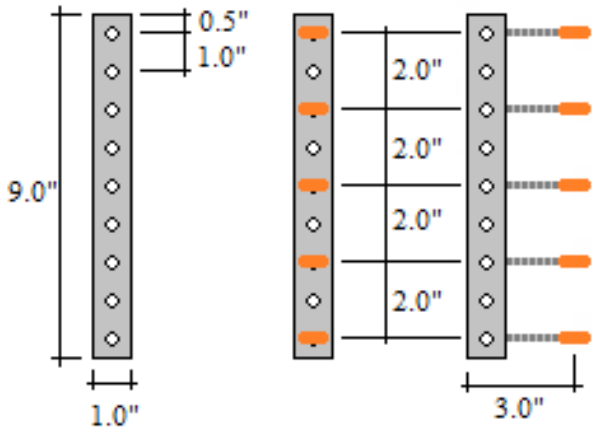

Figure 2-4 Depiction of nine inch tall brackets (left) with half-inch clearance at top and bottom. Sensors (orange) were affixed in regular two-inch increments (right).

2.5.2 Instrumentation of concrete crossties at manufacturing facility

Eleven brackets were installed into seven concrete crosstie molds at the LB Foster CXT Concrete Crossties production facility located in Tucson, AZ. The seven crosstie are uniquely identified as A-444, A-445, A-446, A-447, A-448, A-449, and A-450. Crossties A-444 through A-447 were cast with brackets at both rail seat areas while crossties A-448 through A-450 were cast with brackets at one end only. The location of the sensor at either end of the crosstie is denoted by IDS or USA depending on the location of the identifying stamp number at either end of the crosstie. A schematic of the location of the brackets within the crosstie is shown in Figure 2-5. Each bracket

was directly fastened onto the pre-stressed tendons utilizing zip ties. The bracket was positioned such that the center of the hygrothermal sensors corresponded to the geometric center of the rail seat area. The multi-conductor shielded cabling was routed to the nearest crosstie end where the cables were encased within a threaded PVC access plug. The access plug was firmly affixed onto the bottom surface of the mold such that the cable ends could be easily accessed after de-molding. After de-molding, a cap was added onto the PVC access plug to further protect the cabling ends during monitoring (see Figure 2-6).

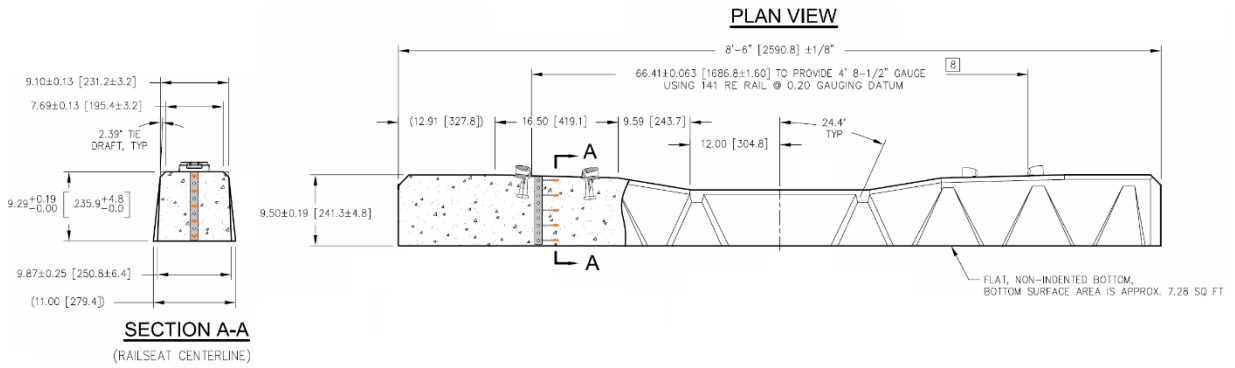

Figure 2-5 Crossties A-448 through A-450 were manufactured with brackets only at one end.

Figure 2-6 De-molded concrete crossties with square cap added to PVC access plug where multi-conductor shielded cables are encased.

The concrete crossties were manufactured no differently from the rest of the plant operations. The approximate concrete mixture design is shown in Table 2-3.

Table 2-3 Approximate concrete mix design of railroad crossties.

Material Type	**Pounds Per Cubic Yard**	**Kilograms Per Cubic Meter**
Type III Portland Cement	650	386
#57 Aggregate	1150	682
#8 Aggregate	750	445
Sand	829	492
Class F Fly Ash	195	116
Water	247	146
Air Entrainer	1.5 fl. oz per 100 lb. cementitious (97.8 mL per 100 kg cementitious)	
High Range Water Reducer	8 fl. oz per 100 lb. cementitious (522 mL per 100 kg cementitious)	

2.5.3 Installation of crossties in model ballast and track

Three of the seven crossties (A-444, A-448, and A-449) were transported to Rantoul, IL, where they were installed inside a model ballast. The model ballast is a 1-1.5 inch top-size yard ballast that conforms to Union Pacific Railroad (UPRR) Class-2 Ballast Specifications. The model ballast and concrete crossties were installed into a 3-compartment box measuring 12-ft by 16-ft and 16 inches in height (see Figure 2-7). Along the 16-ft length, the box was partitioned into approximately 5-ft sections for ease of construction and filling. A level surface of ballast was initially filled into each of the three compartments. The box sits atop an angled asphalt lot, which resulted in one end of each of the compartments being filled with 5 to 6 inches of ballast while the other end was filled with 3 to 4 inches (see Figure 2-8). This angled surface at the underside of the model ballast facilitates rainfall runoff and prevents stagnant water from accumulating within the ballast. Reflective heat from the asphalt lot is minimized with a clearance of 1.75 feet to each end of the crossties from the compartment box edge and an additional distance of 1.9 feet to the instrumented location of the crosstie. This cumulative distance of 3.67 feet is assumed to be sufficiently far from any radiant heat that the asphalt surface may impart onto the underside of the concrete crosstie through 3-6 inches of aggregate ballast. Each crosstie was lifted and positioned into the center of each compartment and seated atop the level ballast. Once the crosstie was positioned, additional ballast was then added in order to reach the top surface of the crosstie. Pads,

clips, and sections of rail line were installed onto the crossties in order to better simulate track conditions.

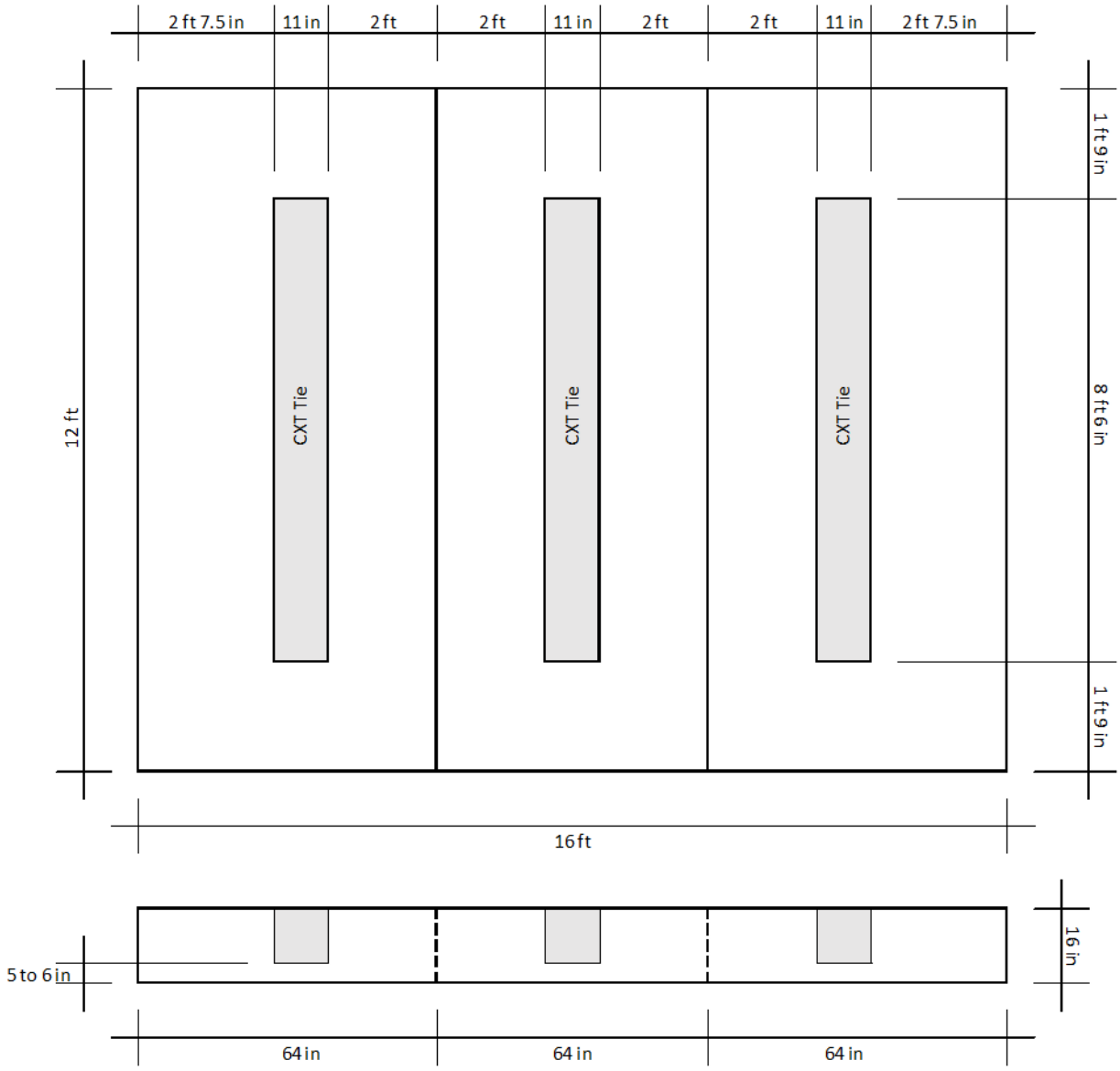

Figure 2-7 Three-compartment model ballast box housing three of the crossties atop yard ballast.



Figure 2-8 Construction of ballast box (left) and final configuration (right).

Publicly available weather information for Rantoul, IL, indicates that there is an average annual snowfall of 37.1 inches and average annual rainfall of 18.2 inches. The average daily high and nightly low temperatures regularly fluctuates between freezing and non-freezing resulting in a relatively high number of freeze-thaw cycles of approximately 80 to 100 [Hershfield, 1973].

The remaining four crossties (A-445, A-446, A-447, and A-450) were transported to a location approximately 10 kilometers south of Lytton, British Columbia, Canada, to be installed in track. The selected track is owned by Canadian National (CN) and runs between Hope, BC, and Lytton, BC, along the Trans-Canada Highway and Fraser River. The four crossties were installed near the Cisco Bridges along track mile markers 103.8 and 104.2 (see Figure 2-9). Additionally, hygrothermal sensors were installed in an electrical conduit box in order to record ambient air temperatures and relative humidity immediately adjacent to the installation site.

Figure 2-9 Google satellite image showing approximate location of four ties installed in track near Cisco Bridges, Lytton, BC.

Publicly available weather information for Lytton, BC, indicates that there is extensive snowfall along this area of the Fraser River valley. Lytton, BC, records an average annual snowfall of 46.22 inches and average annual rainfall of 13.33 inches. The warm season lasts from June 17 to September 9 while the cold season lasts from November 15 to February 19. More importantly, the average daily high and nightly low temperatures regularly fluctuates between freezing and non-freezing from March to May and from September to November. This fluctuating temperature results in a relatively high number of freeze-thaw cycles of approximately 60 to 80 [Fraser, 1959]. After installation in October 2013, research partners at the University of British Columbia, Okanagan, retrieved recorded data every 3 months through March 2015.

2.5.4 Complementary installation of modulus of rupture beams and model concrete crossties in model ballast

Additionally, three instrumented modulus of rupture (MOR) beams measuring 6-inch by 6-inch by 21-inch and two model crossties measuring 9-inch by 9-inch by 16-inches were installed into the model ballast such that their top surface was level with the crossties. The nominal concrete mixture design for these complementary members is shown in Table 2-4. The concrete mix design is intended to be comparable to the concrete crossties installed in track and in model ballast. Each MOR beam was instrumented with 4 hygrothermal sensors positioned 11.5 inches from either end of the beam and at depths of 0.5, 1.5, 4.5, and 5.5 inches, as shown in Figure 2-10. The benefit of these beams is that they are more easily removed from ballast than the crossties in order to re-condition them in an environmentally controlled room whenever necessary. Each model crosstie was instrumented with 4 hygrothermal sensors positioned 8 inches from either end of the length and at depths of 0.5, 2.5, 5.5, and 8.5 inches, as shown in Figure 2-11. Additionally, one model tie was constructed with anchors such that a polyurethane bad and section of rail could be fastened at a later point in time in order to better simulate track environments.

Table 2-4 Nominal concrete mix design of modulus of rupture beams and model crossties.

Material Type	**Pounds Per Cubic Yard**	**Kilograms Per Cubic Meter**
Type I Portland Cement	718	426
#7 Aggregate	2085	1236
Sand	1257	746
Water	216	128
High Range Water Reducer	12 fl. oz per 100 lb. cementitious (782 mL per 100 kg cementitious)	

Figure 2-10 Illustration of 6 x 6 x 21 inch modulus of rupture concrete beam instrumented with hygrochron sensors at depths of 0.5, 1.5, 4.5, and 5.5 inches from the top surface. The sensors are centrally situated in the beam 3 inches from the width of the beam at 10.5 inches from either end. The beams are installed in model ballast in Rantoul, IL.

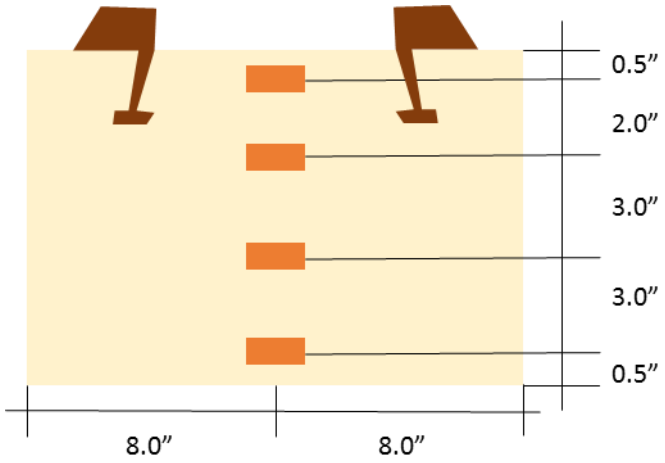

Figure 2-11 Illustration of model 9 x 9 x 16 inch model concrete crosstie instrumented with hygrochron sensors at depths of 0.5, 2.5, 5.5, and 8.5 inches from the top surface. The sensors are centrally situated in the model crosstie approximately 4 inches from the width of the prism at 8 inches from either end. The model crossties are installed in model ballast in Rantoul, IL.

2.6 Results

The instrumented concrete crossties, model crossties, and modulus of rupture beams typified similar behaviors. Namely, hygrothermal sensors functioned appropriately at early ages and failed at later ages. However, the large data set observed over the 1 year period allows for meaningful observations and conclusions to be drawn.

2.6.1 Relative humidity results over observation period

Although relative humidity of ambient conditions fluctuates daily, internal relative humidity of concrete members fluctuate in a more seasonal manner except for the near surface of the concrete surface. Figure 2-12 shows a model concrete crosstie moved from a dry, indoor environment to model ballast in Rantoul, IL, where sensors closer to the exterior surface (0.5 and 8.5 inches) rise in relative humidity value. Internal relative humidity at depths of 2.5 and 5.5 inches remain significantly high and do not respond to the change in environment in a drastic manner. A similar trend is observed in a modulus of rupture beam installed in ballast (see Figure 2-13).

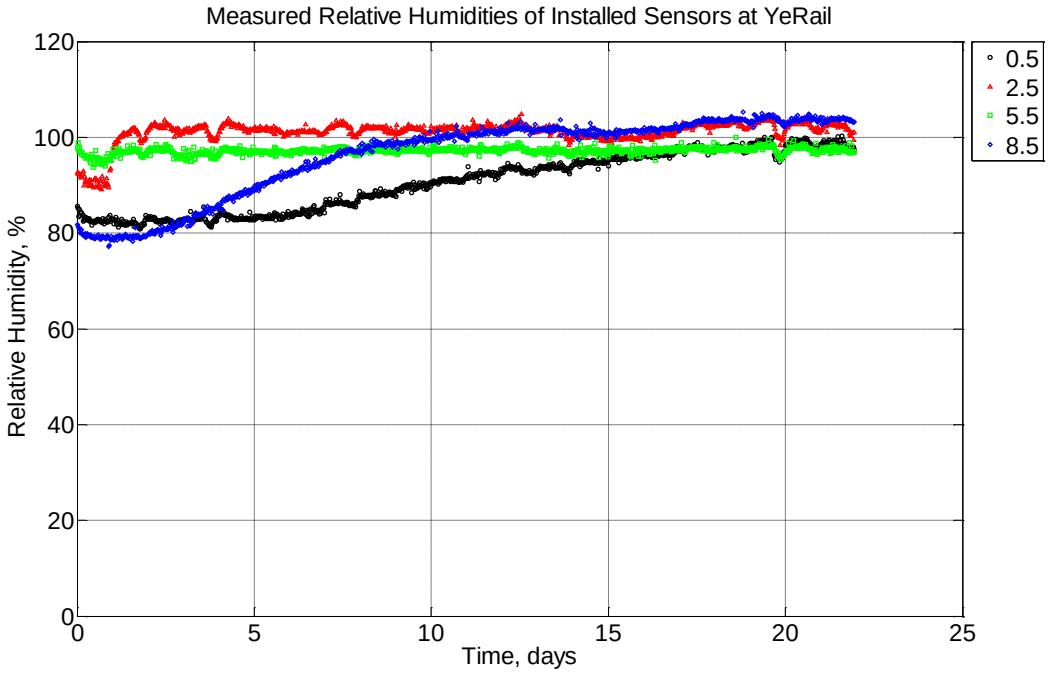

Figure 2-12 Measured relative humidity at depths of 0.5 inches (12.7 mm), 2.5 inches (63.5 mm), 5.5 inches (139.7 mm), and 8.5 inches (215.9 mm) from the surface of a model concrete crosstie (labeled YeRail) installed in ballast in Rantoul, IL, between November 29, 2014, through December 21, 2014. An 8 mm thick polyurethane pad and 12 in (30.48 cm) length 136 lb/yd (67.5 kg/m) section of steel rail are additionally installed atop the model concrete crosstie.

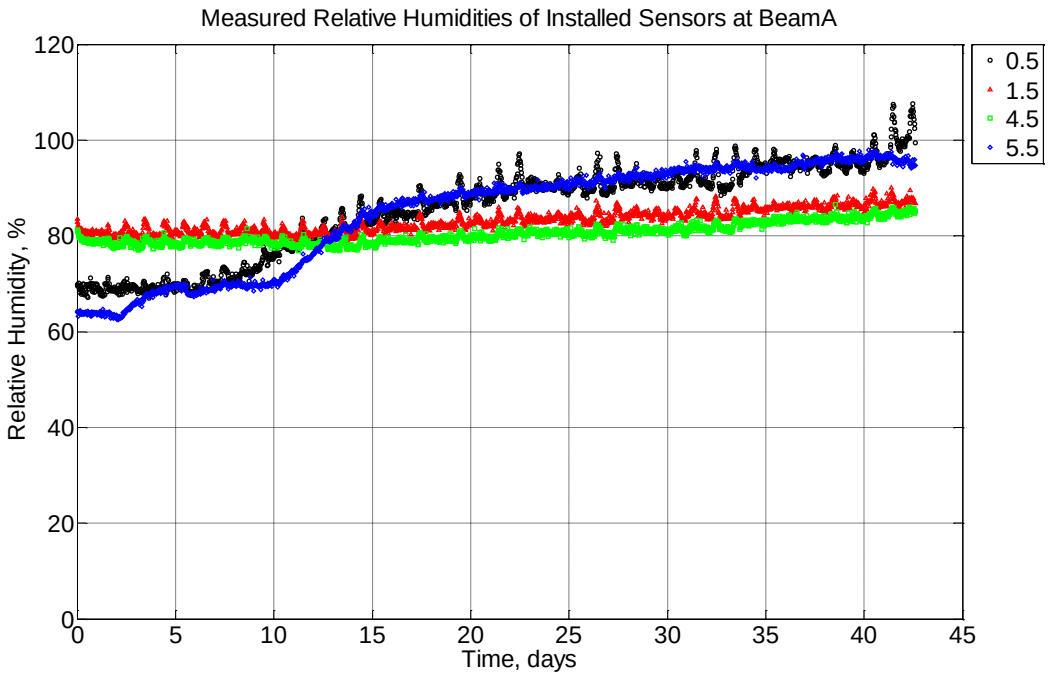

Figure 2-13 Measured relative humidity at depths of 0.5 inches (12.7 mm), 1.5 inches (38.1 mm), 4.5 inches (114.3 mm), and 5.5 inches (139.7 mm) from the surface of a modulus of rupture beam (labeled A) installed in ballast in Rantoul, IL, between October 19, 2014, through November 30, 2014.

Whenever these concrete members were installed in ballast, measureable relative humidity values inside the concrete steadily increased and did not appreciably decrease. In order to confirm that the proposed 1-dimensional relative humidity model is appropriate for the finite-width concrete member in a drying case, the modulus of rupture beams were removed from ballast, on occasion, and moved into an environmentally controlled room where the ambient relative humidity was maintained at 50% relative humidity. The response of the sensors is as expected where internal humidity near the exterior of the concrete surface (0.5 and 5.5 inches) fell more quickly than what was measured at the interior of the concrete member (1.5 and 4.5 inches) (see Figure 2-14).

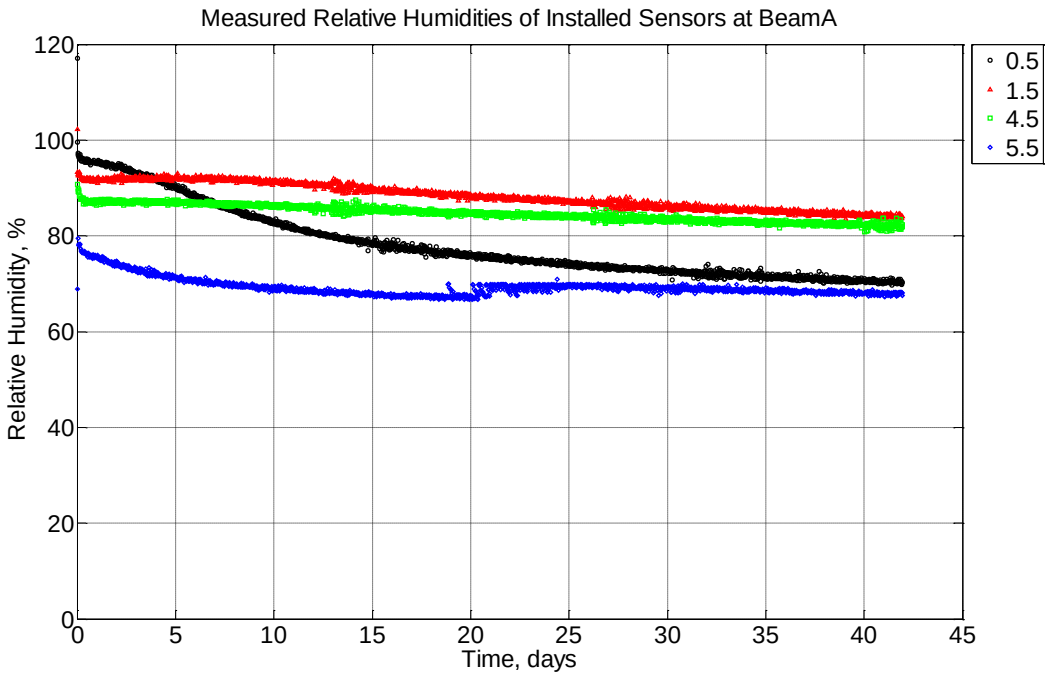

Figure 2-14 Measured relative humidity at depths of 0.5 inches (12.7 mm), 1.5 inches (38.1 mm), 4.5 inches (114.3 mm), and 5.5 inches (139.7 mm) from the surface of a modulus of rupture beam (labeled A) located inside an environmentally controlled room (50% RH, 23ºC) between July 29, 2014, through September 9, 2014.

2.6.2 Temperature results over observation period

Concrete exposed to ambient conditions undergo greater temperature fluctuations than relative humidity fluctuations. Figure 2-15 shows a concrete crosstie installed in track near Lytton, BC, for 85 days in the winter season and Figure 2-16 shows greater detail of fluctuations across 10 days in that same period. Each of its embedded hygrothermal sensors depict wide ranging temperature fluctuations mostly attributable to the daily temperature changes. Moreover, it is observed that fluctuations at the top and bottom of the crosstie will undergo freezing events in a cyclic manner. Figures 2-17 and 2-18 similarly depicts a concrete crosstie installed in model ballast in Rantoul, IL, in the summer months. Similar to Figure 2-16, the daily and daily and nightly fluctuations in Figure 2-18 are more prominently evident because of a shorter observation period. It is worth noting that near the surface of the concrete crosstie, the temperatures will increase to values much higher than the interior of the member. During nighttime temperatures, the concrete crosstie appears to reach comparable values.

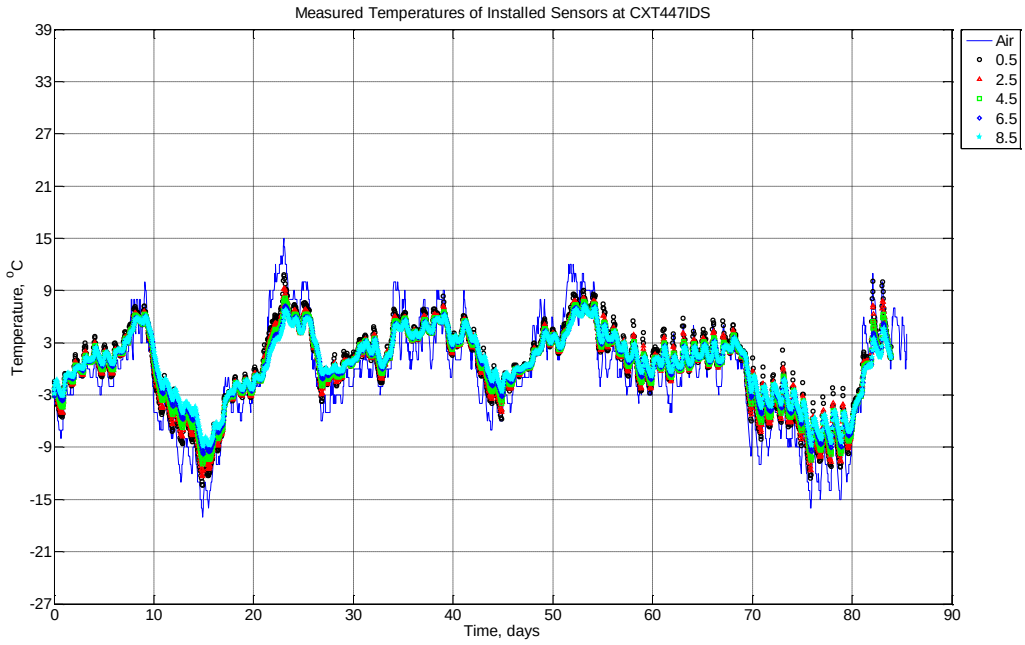

Figure 2-15 Measured air temperature and measured temperature values at depths of 0.5 inches (12.7 mm), 2.5 inches (63.5 mm), 4.5 inches (114.3 mm), 6.5 inches (139.7 mm), and 8.5 inches (215.9 mm) from the surface of a concrete crosstie (labeled CXT447IDS) installed in track near Lytton, BC, between November 22, 2013, through February 14, 2014. An 8 mm thick polyurethane pad and steel rail are additionally installed atop the concrete crosstie.

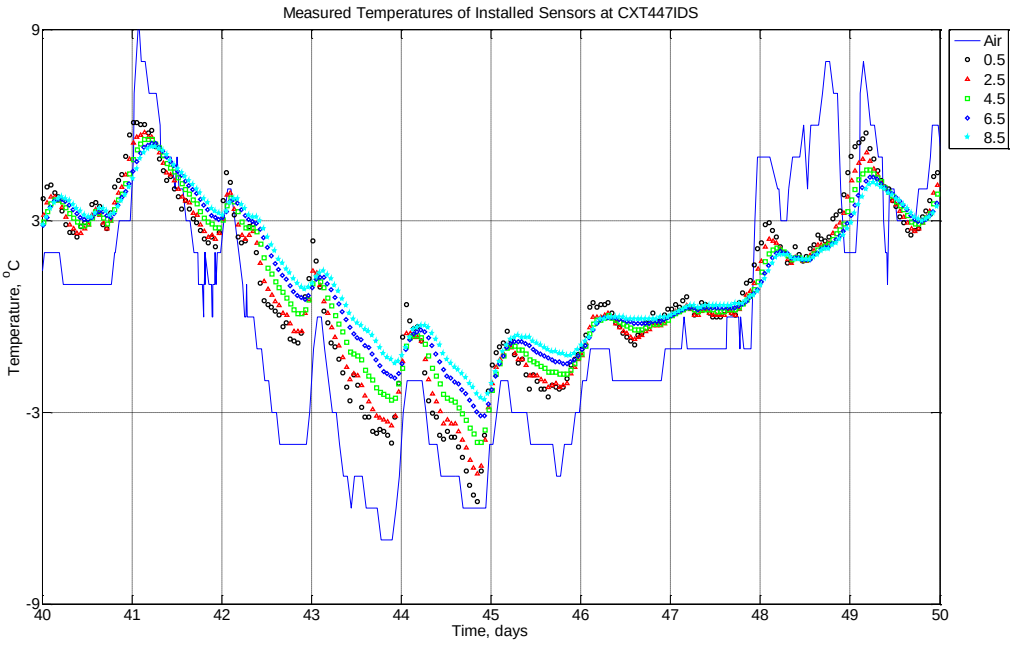

Figure 2-16 Measured air temperature and measured temperature values at depths of 0.5 inches (12.7 mm), 2.5 inches (63.5 mm), 4.5 inches (114.3 mm), 6.5 inches (139.7 mm), and 8.5 inches (215.9 mm) from the surface of a concrete crosstie (labeled CXT447IDS) installed in track near Lytton, BC, between January 1, 2014, through January 10, 2014. An 8 mm thick polyurethane pad and steel rail are additionally installed atop the concrete crosstie.

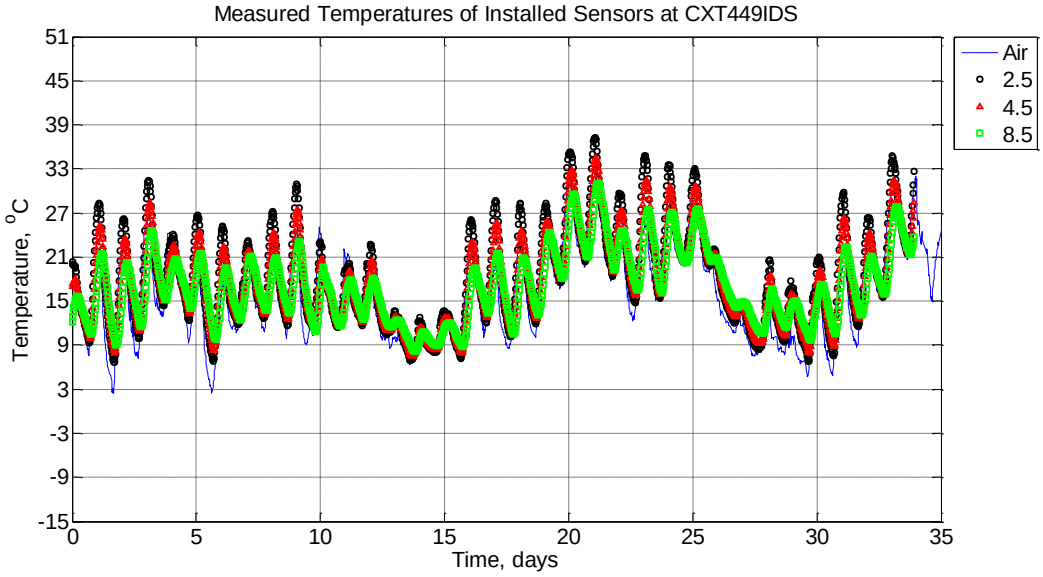

Figure 2-17 Measured air temperature and measured temperature values at depths of 2.5 inches (63.5 mm), 4.5 inches (114.3 mm), and 8.5 inches (215.9 mm) from the surface of a concrete crosstie (labeled CXT449IDS) without a polyurethane pad nor rail installed in ballast in Rantoul, IL, between April 17, 2014, through May 21, 2014.

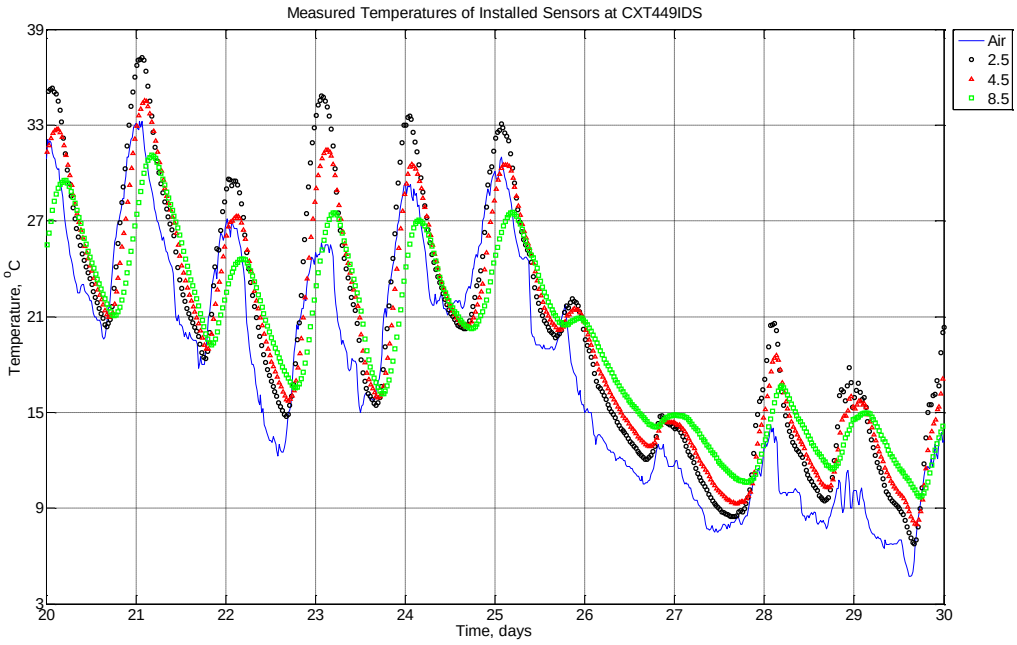

Figure 2-18 Measured air temperature and measured temperature values at depths of 2.5 inches (63.5 mm), 4.5 inches (114.3 mm), and 8.5 inches (215.9 mm) from the surface of a concrete crosstie (labeled CXT449IDS) without a polyurethane pad nor rail installed in ballast in Rantoul, IL, between May 7, 2014, through May 17, 2014.

2.7 Discussion of Results and Predictive Modeling

2.7.1 Internal relative humidity distribution

The predictive 1-dimensional moisture transport equation shown in Equation 2-1 is executed in a Matlab script to predict the relative humidity distribution across the depth of 6 inch (153 mm) or 9 inch (230 mm) depending on whether the concrete sample being analyzed is a modulus of rupture beam or a (model) crosstie. However, other parameters are held near constant throughout the entirety of the analysis, namely because of the similarity of the concrete mixture design. The moisture diffusivity at complete saturation is 0.86×10^{-6} m^2/hr, the regression coefficient is selected as 15, α is 0.05 [Kang *et al.*, 2012], and the bifurcation relative humidity point is 75% RH.

In Figure 2-19, the depth across a model concrete crosstie is depicted with an initial condition where the interior of the concrete sample is saturated while the exterior of the concrete sample is in equilibrium with the surrounding environment (approximately 80% RH). The

surrounding environment is defined as the boundary conditions where externally positioned hygrothermal sensors monitor the ballast conditions. The hygrothermal sensor located at the top surface of the ballast is additionally modified according to Table 2-2. Over the span of 20 days, the model concrete crosstie is subjected to high relative humidity values which leads to its relative humidity values to increase over time. This increase with respect to time is encapsulated by the model (continuous line) moving rightward, not exceeding 100% relative humidity.

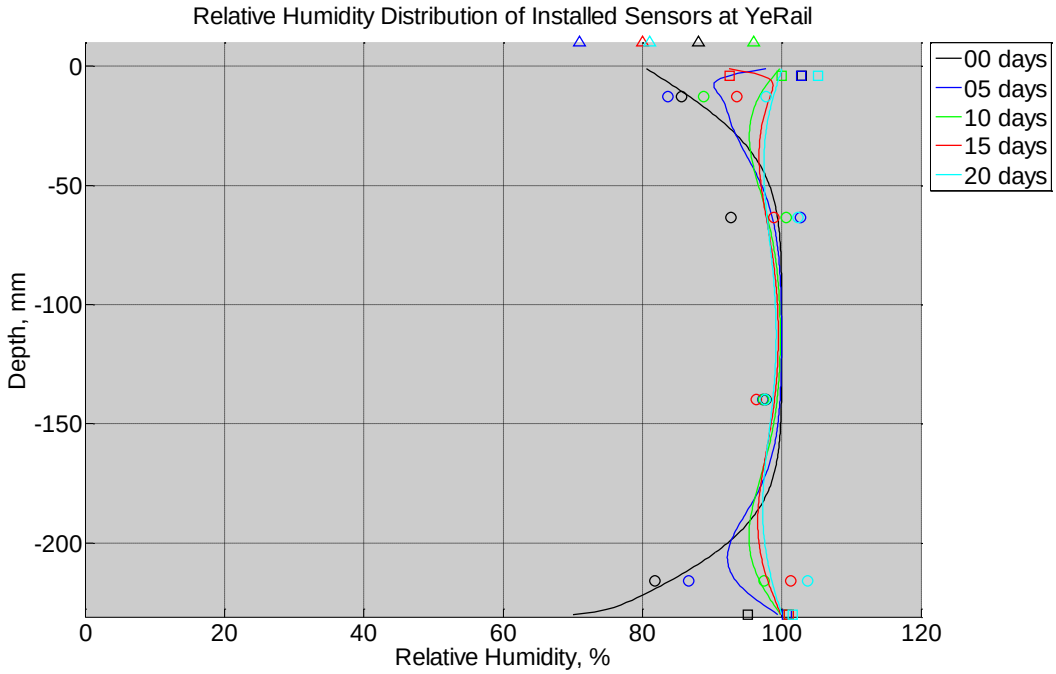

Figure 2-19 Measured (markers) and modeled (continuous line) relative humidity profile distribution as a function of depth inside a model concrete crosstie (labeled YeRail) installed in ballast in Rantoul, IL, between November 29, 2014, through December 21, 2014. An 8 mm thick polyurethane pad and 12 in (30.48 cm) length 136 lb/yd (67.5 kg/m) section of steel rail are additionally installed atop the model concrete crosstie. The model does not incorporate a polyurethane pad nor steel rail line. Triangular markers denote relative humidity value from KTIP weather station, square markers denote measured relative humidity values from ballast, and circular markers denote measured relative humidity values inside concrete.

The predicted values throughout the depth of the model concrete crosstie can be compared against the experimentally determined relative humidity values as measured by the hygrothermal sensors. This comparison produces Figure 2-20 where each point represents a singular moment in time and whose coordinates represent predicted and measured relative humidity values. A perfect prediction of relative humidity values would produce a scatter of data that suitably overlies the

line of equality. Figure 2-20 shows a relatively good agreement between predicted and measured relative humidity values at each of the four depths inside the model concrete crosstie.

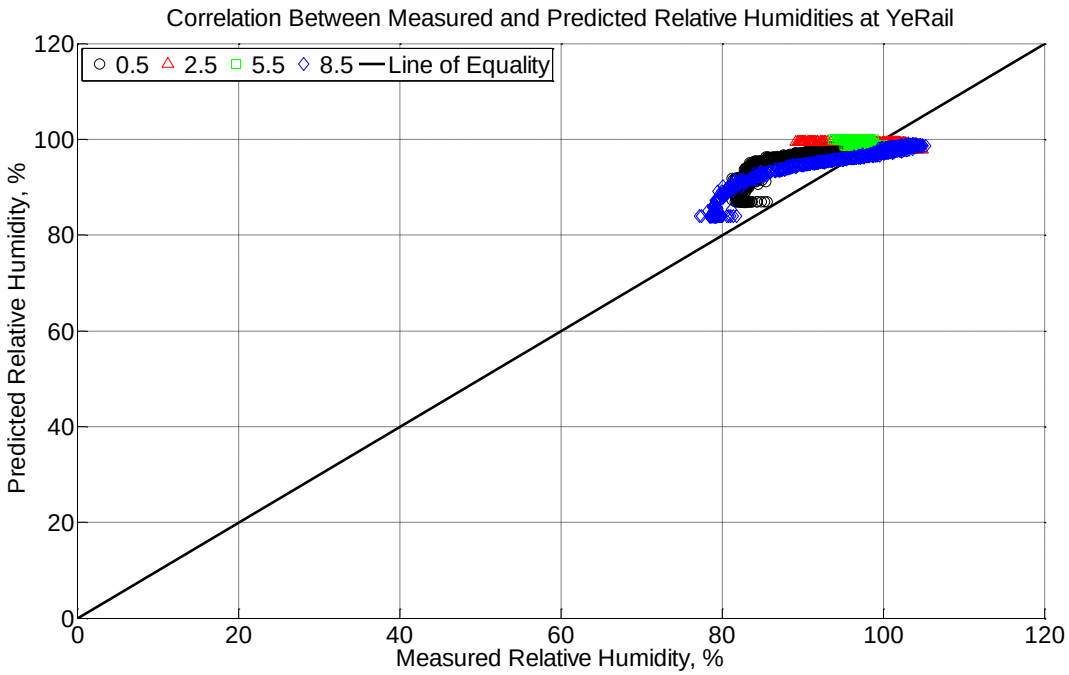

Figure 2-20 Correlation between measured and predicted relative humidity values 0.5 inches (12.7 mm), 2.5 inches (63.5 mm), 5.5 inches (139.7 mm), and 8.5 inches (215.9 mm) from the surface of a model concrete crosstie (labeled YeRail) installed in ballast in Rantoul, IL, between November 29, 2014, through December 21, 2014. An 8 mm thick polyurethane pad and 12 in (30.48 cm) length 136 lb/yd (67.5 kg/m) section of steel rail are additionally installed atop the model concrete crosstie. The model does not incorporate a polyurethane pad nor steel rail line.

The inclusion of modified boundary conditions to reflect moisture becoming entrapped by the polyurethane pad and rail line is not wholly isolated due to the finite-width nature of the model concrete crosstie. Figure 2-21 shows the same predictive model applied to a modulus of rupture beam similarly installed in the model ballast in Rantoul, IL. However, no confining polyurethane pad nor rail line are installed. In this scenario, the modulus of rupture beam is not wholly saturated at the interior at the start of the simulation. However, a similar trend is observed that the modeled line is moving rightward indicating an increase in predicted internal relative humidity. Figure 2-22 compares the predicted and measured relative humidity values to again find a comparably good agreement.

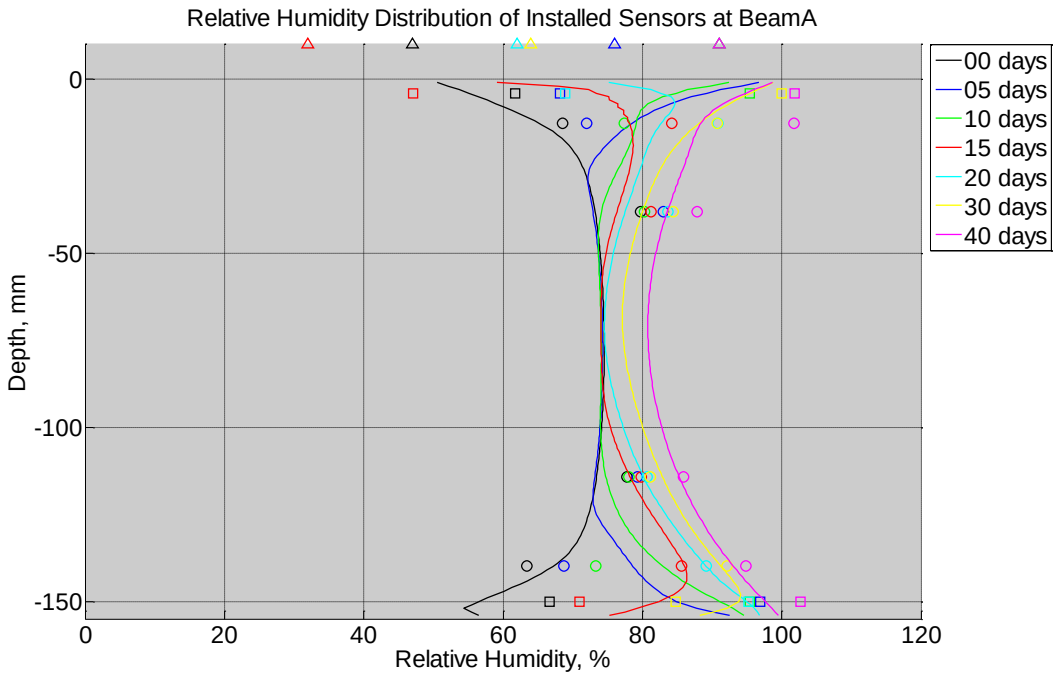

Figure 2-21 Measured (markers) and modeled (continuous line) relative humidity profile distribution as a function of depth inside modulus of rupture beam (labeled A) installed in ballast in Rantoul, IL, between October 19, 2014, through November 30, 2014. Triangular markers denote relative humidity value from KTIP weather station, square markers denote measured relative humidity values from ballast, and circular markers denote measured relative humidity values inside concrete.

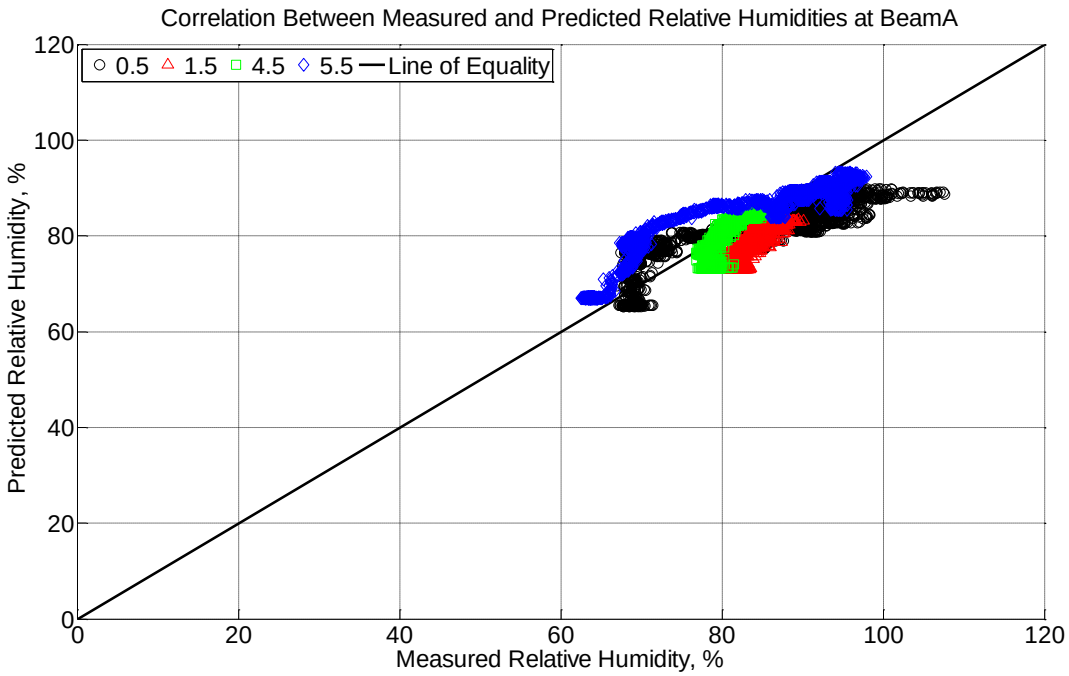

Figure 2-22 Correlation between measured and predicted relative humidity values 0.5 inches (12.7 mm), 1.5 inches (38.1 mm), 4.5 inches (114.3 mm), and 5.5 inches (139.7 mm) from the surface of a modulus of rupture beam (labeled A) installed in ballast in Rantoul, IL, between October 19, 2014, through November 30, 2014.

In these instances of wetting as depicted in Figures 2-12 and 2-13, the predictive moisture transport model is suitable in characterizing the increasing internal relative humidity. In the event of drying, the boundary conditions can be altered to remain constant at both the topside and underside of a modulus of rupture beam when it is moved to an environmentally controlled room. Figure 2-23 shows the predicted change in relative humidity when a nominally saturated concrete modulus of rupture beam is moved into a 50% relative humidity controlled environment. It is evident that the predicted values (continuous line) shifts leftward indicating drying. When these predicted values are again compared to measured values (see Figure 2-24), the good agreement between predicted and measured relative humidity values becomes apparent again.

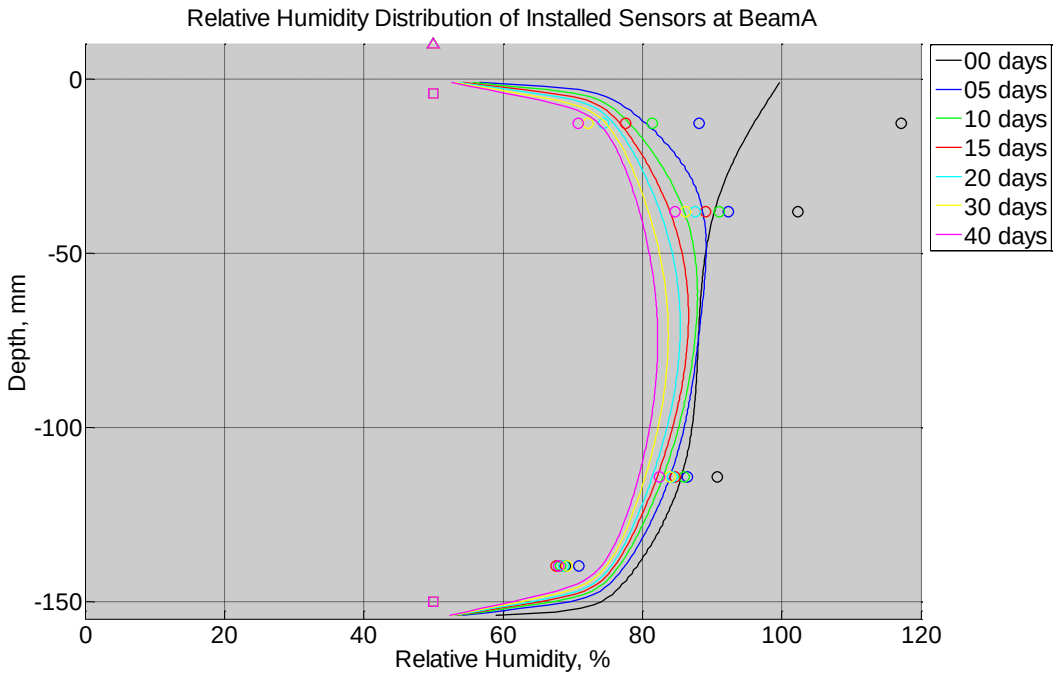

Figure 2-23 Measured (markers) and modeled (continuous line) relative humidity profile distribution as a function of depth inside modulus of rupture beam (labeled A) located inside an environmentally controlled room (50% RH, 23°C) between July 29, 2014, through September 9, 2014. Triangular markers denote relative humidity value from control panel, square markers denote measured relative humidity values from ambient sensors, and circular markers denote measured relative humidity values inside concrete.

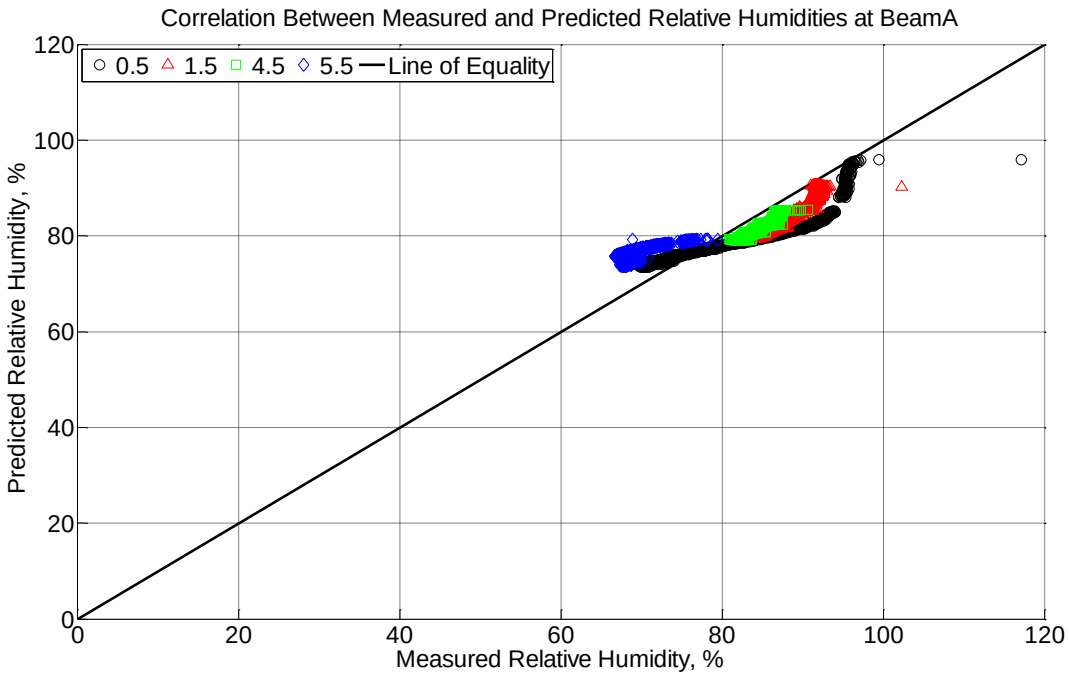

Figure 2-24 Correlation between measured and predicted relative humidity values 0.5 inches (12.7 mm), 1.5 inches (38.1 mm), 4.5 inches (114.3 mm), and 5.5 inches (139.7 mm) from the surface of a modulus of rupture beam (labeled A) located inside an environmentally controlled room (50% RH, 23ºC) between July 29, 2014, through September 9, 2014.

2.7.2 Solar radiation estimation

The solar radiation at a given geo-temporal location must be estimated in order for the predictive 1-dimensional, multi-layered temperature model to work suitably. As such, Equation 2-11 is solved in order to estimate the total incoming solar radiation in Rantoul, IL, and Lytton, BC, throughout the same time period that the predictive temperature modeling is conducted. Figure 2-25 shows the observed temperature and relative humidity in Rantoul, IL, during cool, winter months. In this figure, the estimated solar radiation is relatively low in value. This is sensible due to the shorter length of daytime and increased amount of cloud cover in the winter months. Figure 2-26 shows a similar estimation of the solar radiation in Lytton, BC, during the summer months. Again, the increased estimated solar radiation during this time period is sensible due to lengthier daylight hours and decreased instances of extensive cloud cover.

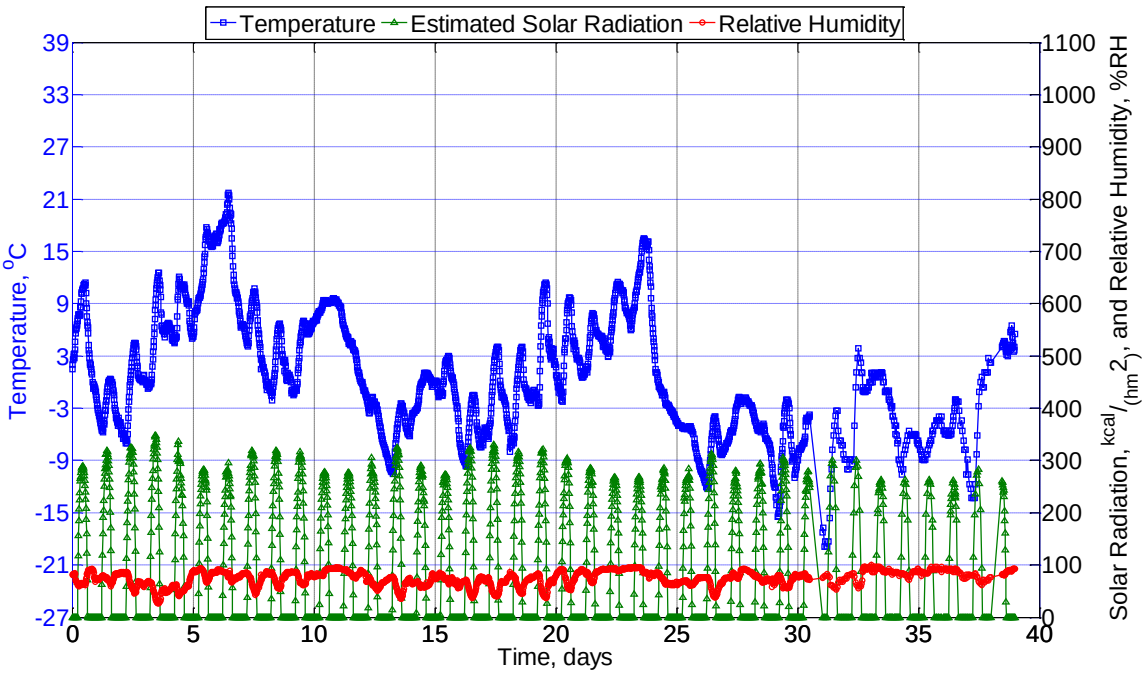

Figure 2-25 Temperature and relative humidity collected from weather station KTIP in Rantoul, IL, from November 12, 2013, through December 18, 2013. Solar radiation is estimated over this same timeframe.

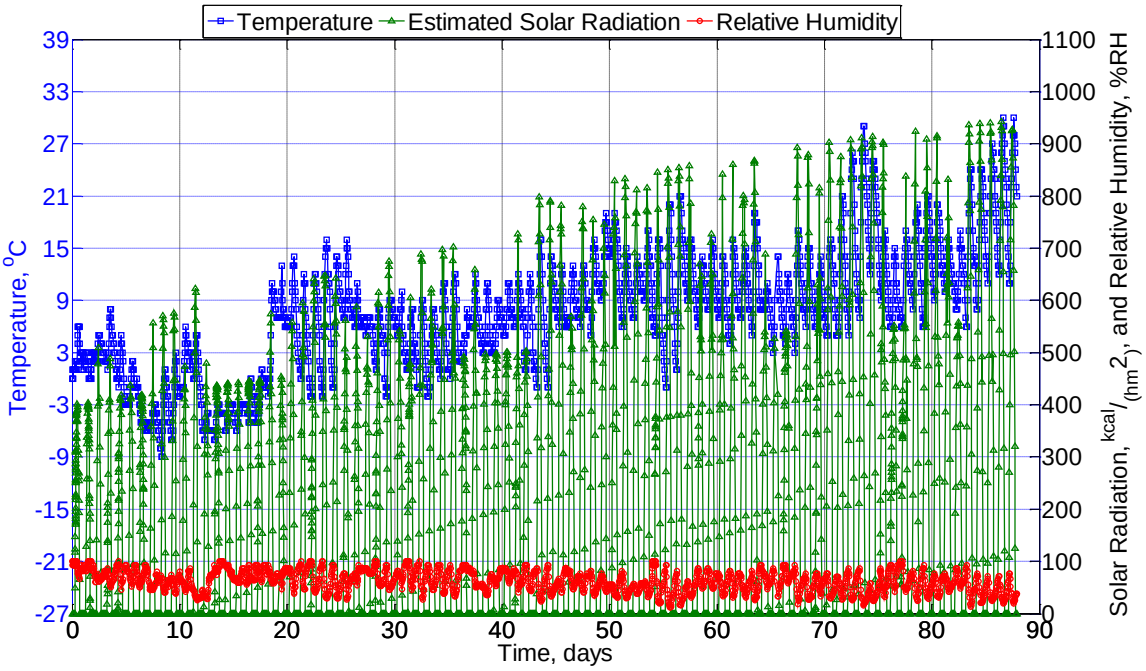

Figure 2-26 Temperature and relative humidity collected from weather station CWLY in Lytton, BC, from February 18, 2014, through May 14, 2014. Solar radiation is estimated over this same timeframe.

2.7.3 Internal temperature distribution

The predictive 1-dimensional temperature equation shown in Equation 2-9 is executed in a Matlab script in order to predict temperature distribution across the depth of a 6 inch (153 mm) or 9 inch (230 mm) depending on whether the concrete sample being analyzed is a modulus of rupture beam or a (model) crosstie. The parameters involved in order to predictively solve the temperature distribution are held constant throughout the analysis. The pavement surface convection coefficient is 16.29 kcal/m^{2}C^o, the effective absorptivity is 0.55 throughout the entire time period, and the thermal conductivities and thermal diffusivities of each material type are defined in Table 2-5.

Table 2-5 Thermal conductivity and thermal diffusivity of material types used in the temperature predictive modeling. Values are adapted from either reference values, [1]Qin and Hiller, 2014, or [2]Prociak *et al.*, 2000.

Material Type	**Thermal Conductivity, λ (kcal/hmC^o)**	**Thermal Diffusivity, α (m^2/h)**
1025 Carbon Steel	31.2480	0.0531
Polyurethane	0.0172	0.0022[2]
Portland Cement Concrete	1.85[1]	0.0025[1]
Aggregate	2.58[1]	0.0030[1]

In Figure 2-27, the predictive model is shown at seven discrete points in time across 90 days of analysis of a concrete crosstie installed in track near Lytton, BC. The only boundary condition inputted into this model are the ambient air temperature at the topside of the concrete crosstie as measured from a nearby weather station and the estimated solar radiation. The multi-layered predictive temperature model is modeled in two manners: with a polyurethane pad and steel rail, or without a polyurethane pad nor steel rail. The results from these two formats is extensively shown in Appendix A4, A6, A8, and A10. It is readily observed that the incorporation of a polyurethane pad and steel rail line does not greatly enhance the predictive fit of the model. This is strongly evidenced in Figure 2-28 where the predicted temperature values are compared against the measured temperature values. In this modeling effort, the correlation between the predicted and measured values is good. This is accomplished despite not incorporating a polyurethane pad nor steel rail line. In an effort to more properly depict the physical thicknesses of the overlying materials, an analysis is performed where the polyurethane pad is constructed with

a thickness of 8 mm while the steel rail line is constructed with a thickness of 10 mm. The result of this fit is shown in Figure A10-42 (in Appendix A) where the increased insulation from the polyurethane pad blunts the effect of the ambient air temperature and the incoming solar radiation.

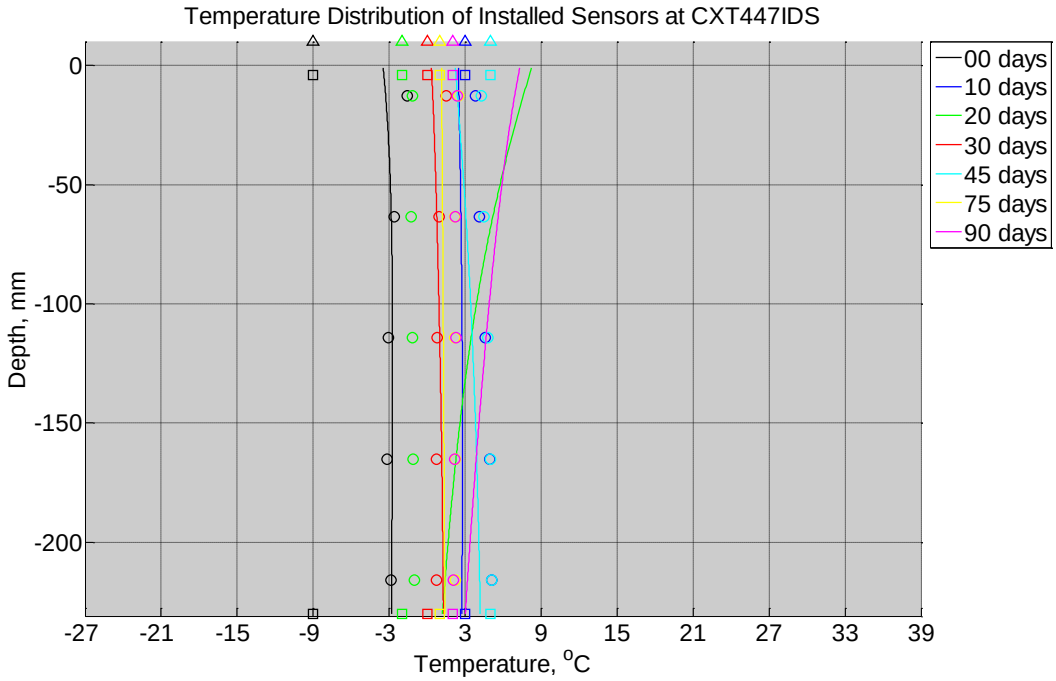

Figure 2-27 Measured (markers) and modeled (continuous line) temperature profile distribution as a function of depth inside a concrete crosstie (labeled CXT447IDS) installed in track near Lytton, BC, between November 22, 2013, through February 14, 2014. An 8 mm thick polyurethane pad and steel rail are additionally installed atop the concrete crosstie. The model does not incorporate a polyurethane pad nor steel rail line. Triangular markers denote temperature value from CWLY weather station, square markers denote assumed temperature values in ballast, and circular markers denote measured temperature values inside concrete.

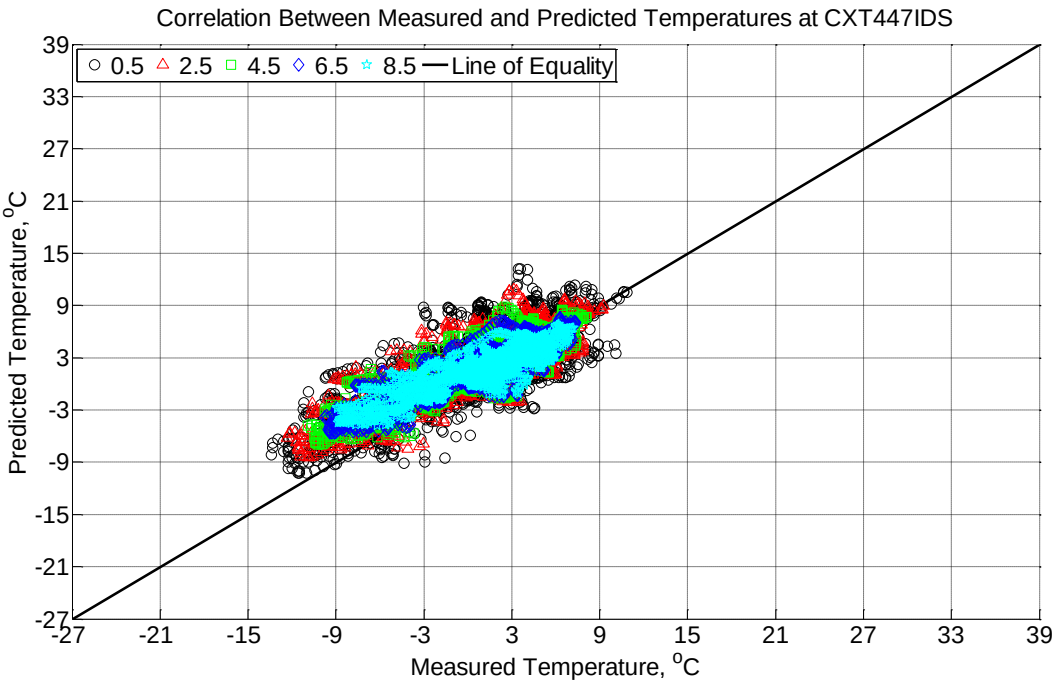

Figure 2-28 Correlation between measured and predicted temperature values 0.5 inches (12.7 mm), 2.5 inches (63.5 mm), 4.5 inches (114.3 mm), 6.5 inches (139.7 mm), and 8.5 inches (215.9 mm) from the surface of a concrete crosstie (labeled CXT447IDS) installed in track near Lytton, BC, between November 22, 2013, through February 14, 2014. An 8 mm thick polyurethane pad and steel rail are additionally installed atop the concrete crosstie. The model does not incorporate a polyurethane pad nor steel rail line.

Figures 2-29 and 2-30 are also predictions of internal temperature, although these depict summer months. Unlike the prediction during wintry months in Figures 2-27 and 2-28, it is evident that the model temperature is over predicted in summer months. This is possible due to a variety of effects. Firstly, the temperature model is reliant upon an estimation of incoming solar radiation. Although the estimation adapted from Spokas and Forcella [2006] is demonstrably good, it is anticipated that there are inherent irregularities with regards to recorded weather when applied to specific instances in time. Passing cloud cover, hazy conditions, and shade from nearby structures potentially obstruct the true incoming solar radiation. Secondly, and of greater importance, is the notion of applying a 1-dimensional pavement model to a 3-dimensional concrete crosstie in ballast. Heat radiation is not occurring linearly through the multiple layers. Instead, heat is transmitting through the layers and is also transmitting through the ballast which is in contact with the side of the crossties. As such, it is likely that an improved model incorporate this additional transference of heat through the aggregate ballast.

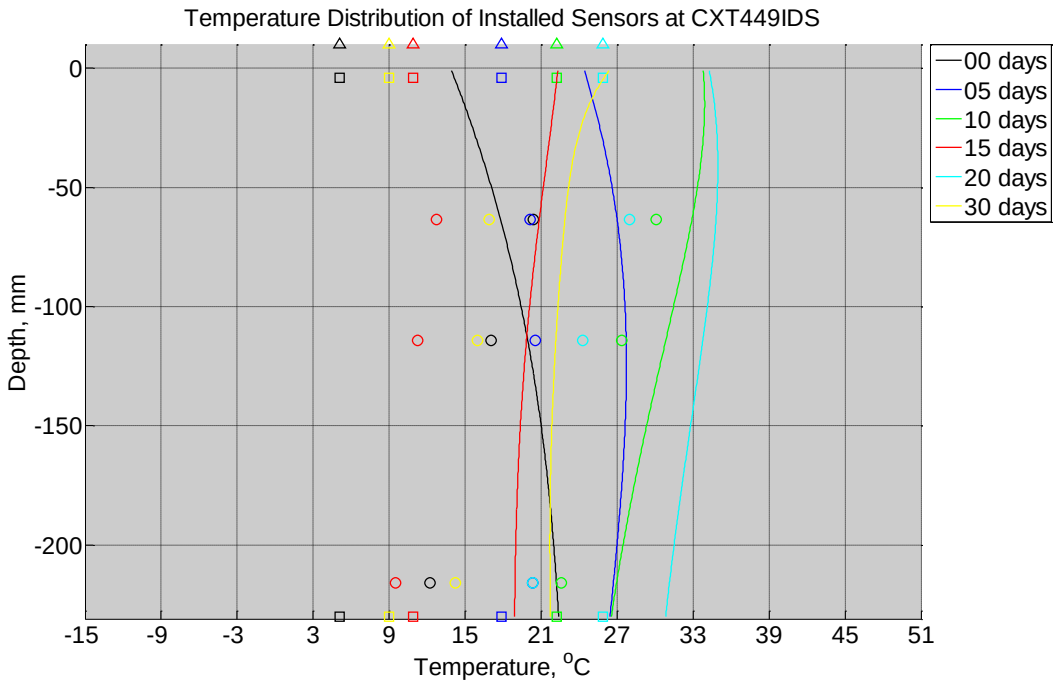

Figure 2-29 Measured (markers) and modeled (continuous line) temperature profile distribution as a function of depth inside a concrete crosstie (labeled CXT449IDS) without a polyurethane pad nor rail installed in ballast in Rantoul, IL, between April 17, 2014, through May 21, 2014. Triangular markers denote temperature value from KTIP weather station, square markers denote measured temperature values from ballast, and circular markers denote measured temperature values inside concrete.

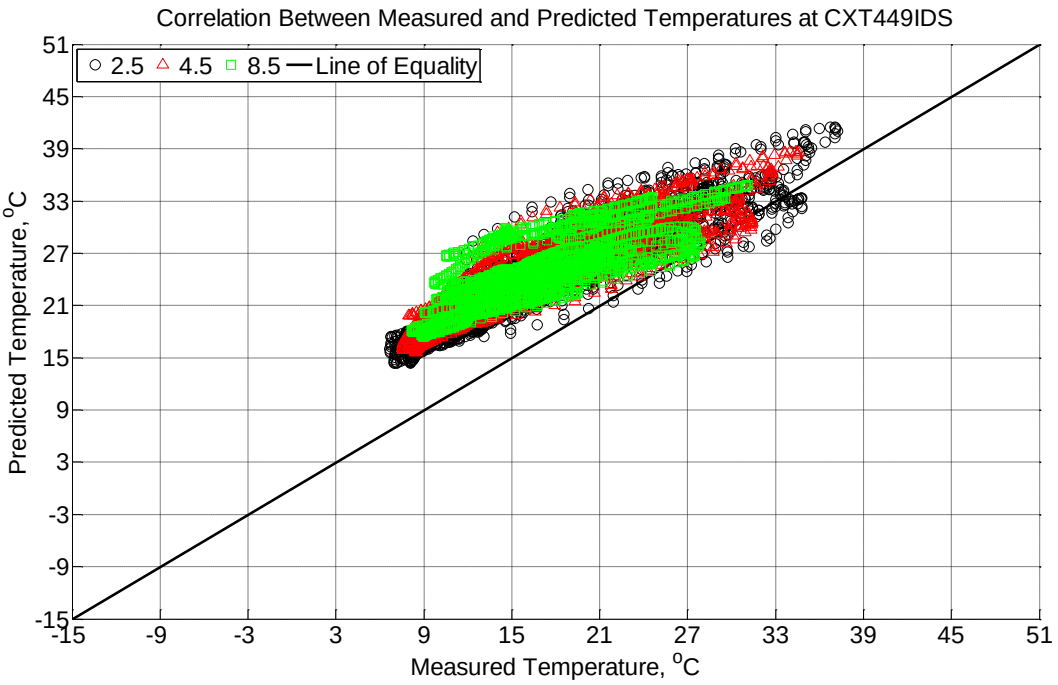

Figure 2-30 Correlation between measured and predicted temperature values 2.5 inches (63.5 mm), 4.5 inches (114.3 mm), and 8.5 inches (215.9 mm) from the surface of a concrete crosstie (labeled CXT449IDS) without a polyurethane pad nor rail installed in ballast in Rantoul, IL, between April 17, 2014, through May 21, 2014.

2.7.4 Effect of ballast conditions

The effect of the ballast acts in two manners upon the concrete crosstie: firstly, it serves as a fast-track avenue for liquid moisture to travel through and (in a well-drained ballast) flow away from the crosstie; secondly, it acts as an additional source of heat transmittance. Both of these factors have an effect on the internal relative humidity and temperature of a concrete crosstie installed in ballast.

Hygrothermal sensors installed in ballast at the topside and underside of a concrete crosstie measured both relative humidity and temperature, depicted in Figures 2-31 and 2-32, respectively. In Figure 2-31, it is evident that the sensor installed at the topside of a crosstie in the ballast undergoes large fluctuations that are comparable to the fluctuations seen in ambient relative humidity measurements. This indicates that aggregates in ballast react rapid to changing moisture conditions and can act as a desiccating force for the concrete crosstie. However, at the underside of the concrete crosstie, it is evident that relative humidity can remain consistently high and near 100% RH. This high relative humidity does not necessarily indicate a poorly drained ballast. It

instead suggests that moisture is trapped within the highly absorptive aggregate and creates a locally humid environment. As a result, this drained, humid ballast acts to slow any drying of the concrete crosstie itself. In large part, this supports the results seen in Figures 2-12 through 2-14 where the internal relative humidity of any concrete member is steadily rising whenever the member is installed within ballast.

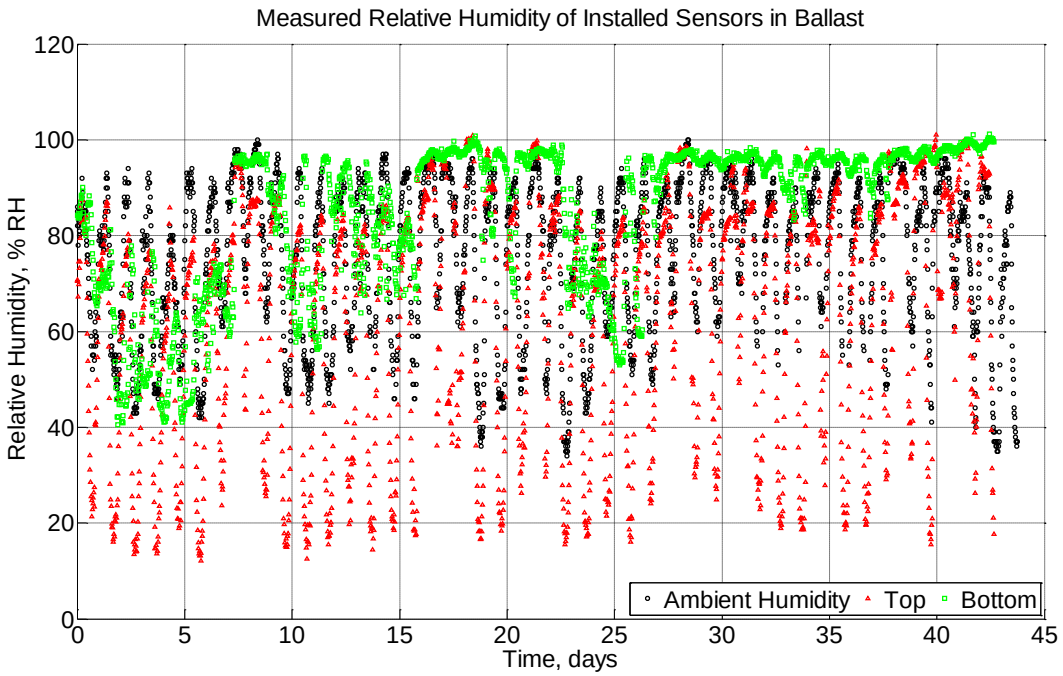

Figure 2-31 Measured relative humidity of model ballast at top and bottom of concrete crosstie in Rantoul, IL, between August 1, 2015, through September 13, 2015. Ambient relative humidity measured from a nearby weather station KTIP is also shown.

Similarly, temperature changes within the ballast are observable in Figure 2-30. At the topside of the ballast, measured temperatures fluctuate to values much higher than ambient air temperatures suggesting that incoming solar radiation is heating the ballast. In turn, this increased temperature immediately adjacent to the concrete crosstie can act to additionally overly increase the internal temperature in the summer months as evidenced in Figure 2-30. At the underside of the concrete crosstie, the hygrothermal sensor installed in ballast shows a muted response due to changing daily temperatures suggesting that the ballast at the underside of the crosstie is partially insulated. While this temperature observation in the ballast may not entirely affect concrete crosstie freeze-thaw resiliency performance, this observation may have an impact on the frost heaving potential of the ballast.

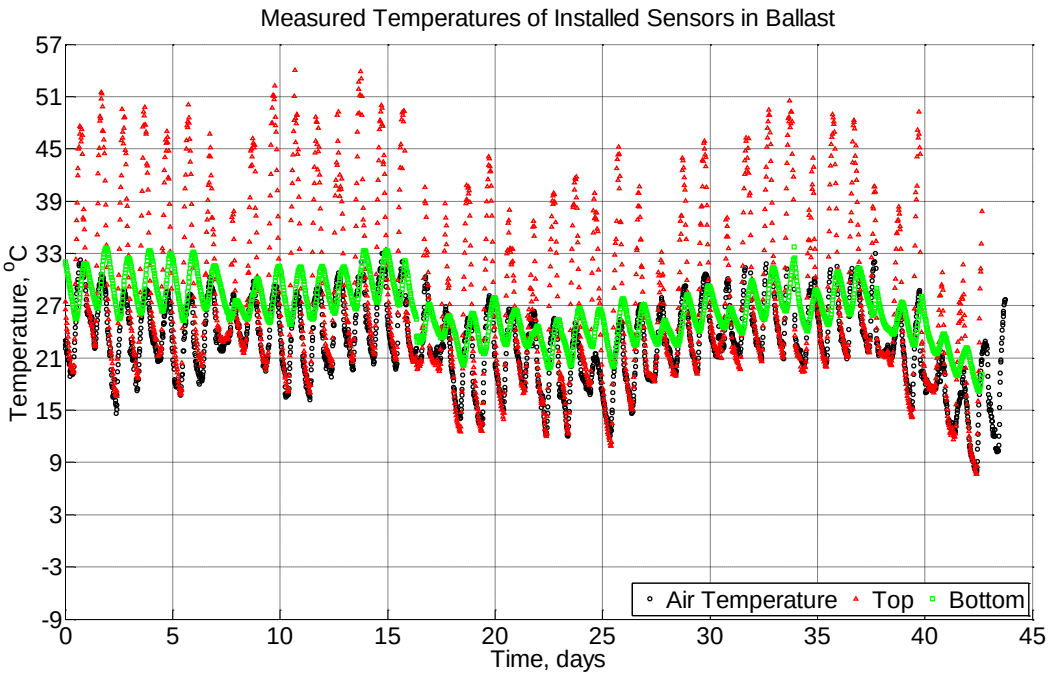

Figure 2-32 Measured temperature of model ballast at top and bottom of concrete crosstie in Rantoul, IL, between August 1, 2015, through September 13, 2015. Ambient air temperature measured from a nearby weather station KTIP is also shown.

2.8 Summary of Chapter

Concrete crossties are subjected to freeze-thaw climates across North America which can lead them to be susceptible to freeze-thaw cyclic damage. Concrete crossties, modulus of rupture beams, and model crossties were instrumented with hygrothermal sensors in order to monitor their internal relative humidity and temperature in two locations: Rantoul, IL, and Lytton, BC. Two 1-dimensional models are applied in order to predict the 3-dimensional response of the concrete crossties in track. It is found that:

- Hygrothermal sensors performed well at early-ages yet failed at later ages. At the time of failure, measured relative humidity values were in excess of 95% suggesting that a combination of persistently high relative humidity, alkalinity from the hydrated cement paste, and possibly high liquid moisture contributed to the material failure of the capacitance film of the hygrothermal sensor. This is indicative, but not definitive, of high moisture inside concrete crossties (modulus of rupture beams, or model crossties) when installed in aggregate ballast.

- A 1-dimensional moisture transport model is adequate to predict the change of internal relative humidity of a concrete member installed in aggregate ballast. The suitability of the model is limited to the geometric center of the rail seat area where the hygrothermal sensors were installed. It is highly likely that the relative humidity closer to the sides of the crossties directly exposed to the aggregate ballast are subject to higher relative humidity values. An improved 2-dimensional (or 3-dimensional) model may better predict the state of internal relative humidity inside a concrete crosstie installed in ballast.
- A 1-dimensional heat transfer model is adequate to predict the change of internal temperature of a concrete member installed in aggregate ballast particularly during wintry months. During this colder time of the year, it is likely that the effect of heat transferring from the immediately adjacent aggregate ballast is minimal. During the summer months, it is found that the model overly predicts the internal temperature. The effect of the polyurethane pad and steel rail is very limited on the predictive temperature model suggesting that a 2- or 3-dimensional model would better serve to predict summer months. In the case of identifying the instances of freezing events, a 1-dimensional pavement model is adequate to predict the 3-dimensional response of a concrete crosstie installed in aggregate ballast. Moreover, the temperature distribution between measured values and predicted values agree well with each where the upper portions of the concrete are more responsive to ambient temperature fluctuations than are interior portions of the concrete. This conclusion, however, is limited to the geometric center of the crosstie at the rail seat area where the study was conducted.

2.9 References

Al Riza, D. F., ul Haq, S. I., and Aris, M. S. "Hourly solar radiation estimation using ambient temperature and relative humidity data." *International Journal of Environmental Science and Development* 2 (2011): 188 – 193.

Barber, E. S., "Calculation of maximum pavement temperatures from weather reports." *Highway Research Board Bulletin* 168 (1957): 1 – 8.

Bakharev, T., and Struble, L. J. "Microstructural features of railseat deterioration in concrete ties." *Journal of Civil Engineering Materials* 9 (1997): 146 – 153.

Bažant, Z., and Najjar, L. "Nonlinear water diffusion in nonsaturated concrete." *Materials and Structures* 5 (1972): 3 – 20.

Bristow, K. L., and Campbell, C. S. "On the relationship between incoming solar radiation and daily maximum temperature and minimum temperature." *Agricultural and Forest Meteorology* 31 (1984): 159 – 166.
Burden, R. L., and Faires, J. D. *Numerical Analysis 7th Ed.* 2001, Pacific Grove, California: Brooks/Cole.
Campbell, G. S., and Norman, J. M. *Introduction to Environmental Biophysics 2nd Ed.* 1998, New York: Springer-Verlag.
Dempsey, B. J., and Thompson, M. R. "A heat transfer model for evaluating frost action and temperature related effects in multilayered pavement systems." *Highway Research Record* 342 (1970): 39 – 56.
Ferdous, W., and Manalo, A. "Failures of mainline railway sleepers and suggested remedies – Review of current practice." *Engineering Failure Analysis* 44 (2014): 17 – 35.
Fraser, J.K. "Freeze-thaw frequencies and mechanical weathering in Canada." *ARCTIC North American* 12 (1959).
Hakon, H. "Frost protection of railway lines." *Engineering Geology* 13 (1978): 505 – 517.
Hargreaves, G. H., and Samani, Z. A. "Reference crop evapotranspiration from temperature." *Applied Engineering in Agriculture* 1 (1985): 96 – 99.
Hershfield, D. M. "The frequency of freeze-thaw cycles." *Journal of Applied Meteorology* 13 (1973): 348 – 354.
Kang, S-T, Kim, J-S, Lee, Y., Park, Y-D, and Kim, J-K. "Moisture diffusivity of early age concrete considering temperature and porosity." *KSCE Journal of Civil Engineering* 16 (2012): 179 – 188.
Kim, J-K, and Lee, C-S. "Moisture diffusion of concrete considering self-desiccation at early ages." *Cement and Concrete Research* 29 (1999): 1921 – 1927.
Leech, C., Lockington, D., and Dux, P. "Unsaturated diffusivity functions for concrete derived for concrete derived from NMR images." *Materials and Structures* 36 (2003): 413 – 418.
Li, W., Pour-Ghaz, M., Castro, J., and Weiss, J. "Water absorption and critical degree of saturation relating to freeze-thaw damage in concrete pavement joints." *Journal of Materials in Civil Engineering* 24 (2012): 299 – 307.
Liu, B. Y., and Jordan, R. C. "The interrelationship and characteristic distribution of direct, diffuse, and total solar radiation." *Solar Energy* 4 (1960): 1 – 19.
Liu, D. L. "Incorporating diurnal light variation and canopy light attenuation into analytical equations for calculating daily gross photosynthesis." *Ecological Modelling* 93 (1996): 175 – 189.
Maxim Integrated. (March 2013). *DS1923 Revision 5*. Retrieved from http://datasheets.maximintegrated.com/en/ds/DS1923.pdf.
McVicar, T. R., and Jupp, D. L. B. "Estimating one-time-of-day meteorological data as inputs to thermal remote sensing based energy balance models." *Agricultural and Forest Meteorology* 96 (1999): 219 – 238.
Monteith, J. L. 1965. "Evaporation and the Environment. In the state and movement of water in living organisms." *Proceedings of the 19th Symposium, Society for Experimental Biology* (pp 205 – 234). Cambridge: Cambridge University Press.
Prociak, A., Pielichowski, J., and Sterzynski, T. "Thermal diffusivity of rigid polyurethane foams blown with different hydrocarbons." *Polymer Testing* 19 (2000): 705 – 712.

Solaimanian, M., and Kennedy, T. W. “Predicting maximum pavement surface temperature using maximum air temperature and hourly solar radiation.” *Transportation Research Record* 1417 (1993): 1 – 11.

Spokas, K., and Forcella, F. “Estimating hourly incoming solar radiation from limited meteorological data.” *Weed Science* 54 (2006): 182 – 189.

Tepponen, P., and Eriksson, B-E. “Damages in concrete railway sleepers in Finland.” *Nordic Concrete Research* 6 (1987): 199 – 209.

Qin, Y., and Hiller, J. E. “Simulating moisture distribution within concrete pavement slabs: model development and sensitivity study.” *Materials and Structures* 47 (2014): 351 – 365.

Wang, D., and Roesler, J. R. “One-dimensional temperature profile prediction in multi-layered rigid pavement systems using a separation of variables method.” *International Journal of Pavement Engineering* 15 (2014): 373 – 382.

Zeman, J. C. “Hydraulic mechanisms of concrete-tie rail seat deterioration.” *University of Illinois at Urbana-Champaign* (2010): MS Thesis.